University of Alberta

Quantification of transport properties in microfluidic porous media

by

Jerry Joseph

A thesis submitted to the Faculty of Graduate Studies and Research in partial fulfillment of the requirements for the degree of

Master of Science

Department of Mechanical Engineering

Fall 2012
Edmonton, Alberta

To my Grandmother, my Parents and my family

Abstract

Quantification of transport properties at pore scale is important for efficient oil extraction, improving fuel cell performance etc. An experimental methodology is developed for calculating permeability and porosity in microfluidic devices that contain structured and unstructured porous media. First, fluid flow experiments are conducted in micro channels with integrated micropillars (MCIPs) that mimic structured porous media and the obtained results are compared with available theoretical predictions. It is also found that the resistance to flow is higher in square arrangement of micropillars than in staggered arrangement. Second, experiments are conducted in micro channels containing realistic reservoir pore networks etched in silicon. Analogous to real reservoirs, it is found that the permeability increases with porosity and the flow resistance decreases with increase in Darcy number. Finally, a Monte Carlo based simulation technique is provided for determination of effective gas diffusivity by using realistic images of such unstructured porous media.

Keywords: Porous media, microfluidics, permeability, porosity, pressure drop.

Acknowledgements

I would like to thank my supervisor, Dr. Sushanta Mitra, for his constant support and guidance during the course of last two years. He has been very supportive and has always been a source of rich and varied subject knowledge as well as inspiration. His patient understanding and cooperation in technical manuscript writing processes is something worth emulation. It was a privilege for me to work with him and to gain rich and varied perspectives about engineering research.

I am indebted to Naga Siva Kumar Gunda, PhD candidate, for his wonderful mentoring and constant support during the course of my research. The depth and breadth of his knowledge, dedication to ethics and versatility in research have always been an inspiration which helped me to wade through the work. His timely inputs, both technical and philosophical, have enriched the two years experience which I spent in my research. It was indeed a great pleasure working with him.

I also thank my colleagues and group members in micro and nano scale transport laboratory (MNTL) with whom working for the last two years was a great experience. Their helps, discussions and assistance have greatly helped me in my course and research work.

I acknowledge the financial support received from Natural Sciences and Engineering Research Council (NSERC) of Canada for my research.

Most importantly, I thank my parents and my family for their continued trust and faith in me. Last two years would have been miserable if it was not for their love, prayers and support. I am thankful to them for supporting me in all aspects of life and for being such wonderful people in my life. I am highly indepted to them for their sacrifices for me.

Last but not the least, I thank GOD Almighty for all the help.

Table of Contents

[1] A version of this chapter has been submitted for publication in *Microfluidics and Nanofluidics*, August 2012, *In review*

[2]A version of this section has been published in the *Proceedings of the 10th International Conference on Nanochannels, Microchannels and Minichannels ICNMM 2012, July 8-12, 2012, Puerto Rico, USA*

[3]A version of this section has been submitted for publication in *Lab on a Chip*, September 2012, *In review*

[4]This appendix has been included as supplementary material for chapter 3 which is submitted for publication in *Microfluidics and Nanofluidics*, August 2012, *In review*

[5]This appendix has been included as supplementary material for chapter 3 which is submitted for publication in *Microfluidics and Nanofluidics*, August 2012, *In review*

List of Tables

List of Figures

Chapter 1

Introduction

1.1 Motivation

Understanding fundamental pore scale flow phenomena has been an area of deep interest for researchers in the fields of oil extraction, earth science, life sciences and hydrology, to name a few. The importance of relating the transport properties of the porous media to their internal pore structure is widely known to the researchers in such fields. For example, transport properties such as permeability, relative permeability, capillary pressure etc. depend upon such internal small pore structures and need to be determined for various applications. Thus the necessity to understand the fundamental flow phenomena that takes place at micro and nano scales in such porous media has become imperative. With advances in micro-fabrication technology, fabrication of microfluidic devices is possible through which representation of such small pore structures is possible. At the same time, advances in imaging technology has the ability to extract the pore network information (Hove et al., 1987; Wellington and Vinegar, 1987; Gunda et al., 2011a) from actual porous media which can be transferred onto microfluidic devices using advanced microfabrication techniques. Microfluidic devices that mimic porous media in such small length scales have found uses in commercial applications like microfiltration and micro heat exchangers. The main motivation for this work are the benefits of quantifying various transport properties that are related to flow mechanisms in such microfluidic porous media. Knowledge of transport properties at such small length scales would govern future forays into designing and building more such miniaturized devices with imortance in practical engineering applications.

1.1.1 Problem Definition

This thesis tries to experimentally quantify the flow properties of porous media that are built on microfluidic devices. These porous media, fabricated using state-of-the-art micro fabrication techniques, are representatives of emerging microfluidic porous media used in many engineering applications. It is important to obtain quantitative information about the transport properties in such microfluidic porous media for better optimization of their design, build and use. Also, experimentally quantified flow properties can be used for parameter estimation of microfluidic porous media which serves as an important tool for modelling flow and transport. It has been found that the characterization of porous media at very small length scales (microns) has facilitated the understanding of the transport phenomena better because of the knowledge of the pore level transport mechanisms (Blunt, 2001; Blunt et al., 2002). Hence, porous media have been subjected to precise characterization for understanding the fundamental pore level mechanisms. For example, improvement of enhanced oil recovery (EOR) processes can be attained by studying mechanisms such as capillary pressure, wettability, relative permeability etc. at the pore level which define the flow behavior in such porous media (Blunt, 1997, 1998; Van Dijke et al., 2010). Microfluidic devices that contain structured porous media, such as array of cylindrical micro pillars, have been used in engineering applications like micro filtration, micro pumping, compact heat exchangers. Though these microfluidic devices have been pegged as pioneering technology for applications in many industrial and engineering processes, their application as such would be limited if the basic transport properties are not quantified. For any porous media, two important properties are permeability and porosity. Knowledge of these basic transport and geometric properties at such small length scales would help to quantify the microfluidic porous media and would provide a foundation for future studies related to quantitative modelling of fluid flow in microfluidic porous media. The pressure drop generated in such porous media would also help understand the resistance to fluid flow offered in the porous media that are fabricated at small length scales. With an understanding of the basic transport properties such as permeability and geometric properties such as porosity, the novel microfludic porous media devices can be used better for studying flow and transport mechanisms with applications to oil extraction and revovery, drug transport, filtration, micro

cooling, micro pumping, micro heat exchangers etc.

1.2 Structure of the Thesis

This thesis is divided into five chapters. This first chapter presents the motivation and the problem statement of this research. Chapter 2 presents a literature review of earlier research in : efforts in representing porous media for studying pore scale phenomena using models that contained pore scale information, characterization of porous media in such small scale devices and quantification of transport properties in such small scale devices that contain porous media. Chapter 3 presents the detailed study of experimental pressure drop measurements in structured porous media that consist of microchannels with micropillars. A description of the fabrication, experimental set up and the results of the experimental study are provided in the chapter. Chapter 4 describes the determination of transport and geometric properties in unstructured porous media contained in microfluidic devices. The unstructured porous media consists of networks of pores and throats etched onto silicon. These networks of pores and throats mimic the actual pore networks found in oil bearing rocks. Also, a numerical simulation approach is presented that can be used for determining effective transport properties in unstructured porous media at small length scales using realistic porous media images. Finally, chapter 5 summarizes the key findings of this research and possible pathways of future research.

References

M.J. Blunt. Effects of heterogeneity and wetting on relative permeability using pore level modeling. *SPE Journal*, 2(1):70–87, 1997.

M.J. Blunt. Physically-based network modeling of multiphase flow in intermediate-wet porous media. *Journal of Petroleum Science and Engineering*, 20(3-4):117–125, 1998.

M.J. Blunt. Flow in porous media-pore network models and multiphase flow. *Current Opinion in Colloid and Interface Science*, 6:197–207, 2001.

M.J. Blunt, M.D. Jackson, M. Piri, and P.H. Valvatne. Detailed physics, predictive capabilities and macroscopic consequences for pore-network models of multiphase flow. *Advances in Water Resources*, 25:1069–1089, 2002.

N.S.K. Gunda, B. Bera, N.K. Karadimitriou, S.K. Mitra, and S.M. Hassanizadeh. Reservoir-on-a-chip (roc): A new paradigm in reservoir engineering. *Lab on a Chip*, 11(22):3785–3792, 2011.

A.O. Hove, J.K. Ringen, and P.A. Read. Visualization of laboratory corefloods with the aid of computerized tomography of x-rays. *SPE Reservoir Engineering (Society of Petroleum Engineers)*, 2(2):148–154, 1987.

M.I.J. Van Dijke, M. Lorentzen, M. Sohrabi, and K.S. Sorbie. Pore-scale simulation of wag floods in mixed-wet micromodels. *SPE Journal*, 15(1): 238–247, 2010.

S.L. Wellington and H.J. Vinegar. X-ray computerized tomography. *JPT, Journal of Petroleum Technology*, 39(8):885–898, 1987.

Chapter 2

Literature Review

The previous chapter discussed about the significance of microfluidic devices that contain porous media which can be used for important engineering applications. It also described the importance of quantifying the transport and geometric properties of such microfluidic porous media. In this chapter, different studies related to pore scale transport phenomena and their quantification are discussed. Also, the significance of such studies in various fields and the progress of such studies with the advances in micro fabrication and Micro Electro Mechanical Systems (MEMS) are discussed. Emphasis is placed on discussing the works that focused on quantifying the transport and geometric properties of such porous media and also on the relevance of such porous media with reference to their proximity to practical applications. A close scrutiny of such works is done and a scope for further efforts in representation and quantification of microfludic porous media is identified.

2.1 Flow through porous media

Flow through porous media has been extensively studied in the past for its widespread application in energy and environmental applications (Mason et al., 1967; Millington, 1959; Muskat, 1945; Nam and Kaviany, 2003; Wen et al., 2012; Whitaker, 1966). Areas like oil and gas recovery (Al-Wahaibi, 2010; Barta and Hepler, 1988; Zendehboudi et al., 2011), hydrogen fuel and biofuel cells (Nam and Kaviany, 2003; Wen et al., 2012), underground water and pollutant transport (Simmons, 1982; Soo and Radke, 1984) have greatly advanced due to insights gained through research in porous media transport phenom-

ena. Oil and gas flows in reservoir rocks is a typical and most widely known example of flow through porous media due to its significance in meeting world energy demands (Barenblatt et al., 1990; Dharmadhikari and Kale, 1985; Ene and Polisevski, 1987; Lenormand and Zarcone, 1988; Soo and Radke, 1986). Though work is under progress to find alternative sources to fossil fuels, the world will still continue to use non renewable energy resources to fund its economic growth in the 21st Century (Fanchi, 2000). Majority of the heavy/-light oil is found in natural reservoirs (porous media) and they consist of solid matrix and pore spaces. These natural reservoirs contain random network of these pores which makes the study of flow through them more challenging. A great level of research is currently under way to find new ways of efficient oil and gas extraction from the available resources (Kharrat, 2009; Marle, 1981; Trivedi and Babadagli, 2009; Yadali Jamaloei et al., 2012; Smith and Fleming III, 1980). It is beleived that the key driver to displace oil from the reservoir relies on the fact that the oil-water-gas co-exist in the pore-space of the reservoir and one needs to adopt suitable mechanisms to destabilize the oil from the pore space (Blunt, 2001; Blunt et al., 2002; Jamaloei and Kharrat, 2010; Koplik and Lasseter, 1985; Van Dijke et al., 2010). This brings to the focus, the importance of pore scale studies in porous media which also determines the success of various secondary and tertiary oil extraction methods that involves interaction between various phases like oil, water and gas in such small pore spaces (Dawe, 1990; Manlowe and Radke). Need less to say, properties like porosity and permeability play major role in determining the efficiency of the various secondary and tertiary oil recovery processes in such reservoir rocks. Hence it is important that an effective analysis be done to understand the transport phenomena in such small pore spaces in which the natural oil recovery applications occur. This would help understand the importance of various parameters that influence the fluid flow mechanisms in such small lengths scales.

Transport of underground fluids is another example of critical importance involving porous media. Researchers have tried to understand the transport of water and contaminants in the underground rocks by doing intensive studies of fluid flow in fractured rocks . Application of such research has immense importance in improving the underground water quality and also in improving the flow of water into the water table (McDowell-Boyer et al., 1986; Tang

et al., 1981). As with the case in porous media flows, it is important to understand the pore structure and pore scale flows in such fractures to gain a better understanding of water and pollutant transport in such porous media (Dagan, 1986). In general, understanding of fundamental pore level processes would benefit in creating better and efficient technology that can be used in numerous applications that contain fluid flow through porous media.

2.2 Small scale representation of porous media

Experimental studies have been carried out in the past on both actual porous media samples such a rock core as well as porous media analogs such as random pack of spheres (Zhang and Sun, 2011)or random arrangement of fibres (Kyan et al., 1970). Studies done in actual rock cores help in simulating actual reservoir phenomena but visualization and understanding of fundamental pore level mechanism in such studies is quite difficult. On the other hand, porous media constructed using idealized geometry tend to loose the realistic attributes (geometry, surface properties) of a porous media and hence the flow study results do not match practical applications. Thus a different kind of model was required that could aid in pore scale studies of transport in porous media. Researchers have tried to understand such fundamental pore level mechanisms of fluid transport in porous media by creating miniaturized devices, known as micromodels, that mimicked the porous media in small length scales (Dullien et al., 1986; Grogan and Pinczewski, 1987; Manlowe and Radke, 1966; Owete and Brigham, 1987; Pereira, 1996). They conducted experimental investigations in such micromodels to understand the various transport properties at the fundamental scale which is the pore scale. These micromodels, which consisted of porous media representations etched on glass or epoxy in the past, have been instrumental in the visualization and analysis of single and multiphase flow in porous media.

First attempts on micromodel approach of representing porous media were attempted by Mattax and Kyte (1961) who used only rectangular array of throats (without pores) to represent the porous media. Though highly idealistic representation in terms of actual porous media geometry, they used this

micromodel to study various transport properties like wettability, residual oil saturation and relative permeability. Chen (1985) used micromodels that were created by etching randomly sized pores and throats into transparent epoxy resin. They used the micromodel for studying two-fluid transport phenomena (air and liquid) for studying immiscible fluid displacement processes such as imbibition and drainage in small pores. The uncertainty in the actual dimensions of the pores and throats obtained by the process of etching on epoxy resin is high and hence precise control of the dimensions is not possible. Similarly, Lenormand and Zarcone (1985) studied immiscible fluid displacements in porous media by fabricating micromodel that contained networks etched on transparent polyester resin which also contained uncertainties due to fabrication in polyester resin.

Campbell (1985) conducted high pressure CO_2 flooding experiments to study miscible displacements in micromodels that consisted of circular pores connected by throats etched in glass plates. Though certainly advantageous when compared to the fabrication on resins, they too reported the shrinking of pores during the process of the fabrication in glass and the actual dimensions could only be reported as approximate values. Morrow et al. (1986) used micromodels consisting of pores and throats etched into glass for studying displacements in strongly water-wet cores and also in mixed wet conditions. They reported improved oil recovery from pore bodies with oil trapping in pore throats and used micromodels etched in glass to conduct this study. Soll et al. (1993) also used micromodels that were obtained by etching channels into glass. The void space consisted of circular pore bodies which were connected to their nearest pore bodies by means of narrow channels (throats). These pore bodies and throats were arranged in a square lattice fashion. They used the micromodel for studying three fluid transport phenomena(water, air and oil) for understanding capillary pressure relationships at pore scale. They too acknowledged the variations between the specified and the actual dimensions of the glass micromodel obtained by chemical etching process. Wan and Wilson (1994), Nguyen and Clarence (1993) etc. have also studied a number of transport phenomena which took into account the underlying pore level mechanisms. Their micromodels too consisted of pore networks etched on glass models. Fadaei et al. (2011) did the CO_2 diffusivity measurements as recently as 2011 in micromodels that consisted of channels etched into glass.

One of the important and useful models for realistic pore scale representations of porous media in such micromodels is known as the pore network model. The concept of network representation of porous media was introduced by Fatt (Fatt, 1956a,b,c). Since then, this model has been used in many cases of porous media studies that tried to understand pore scale flow mechanisms. In the pore network model, the bonds are referred to as throats and the nodes are referred to as the pore bodies (void spaces) found in real porous media. Though the network model can fairly be an ordered representation, there can be random network of pores and throats as well that can be used to account for the inherent randomness associated with the porous media. Researchers have since then used the network model representation for two phase and three phase fluid flow studies in porous media. For example, Mani (1998) used network model representations to understand the relative permeability in three phase fluid flow in porous media. Dixit (1999) and Blunt (1998) extended the applications of the network model representation for studying oil recovery processes. Further processes to realistically represent the porous media structure using network models have been investigated (Dong, 2009) which help in mimicking the field scale transport phenomena in porous media.

2.3 Microfluidic porous media

The microstructure of the porous media varies greatly based on applications-natural oil and gas reservoirs have complex pore structures ranging from nanometer to micron sizes (Bera et al., 2012); gas diffusion layer (GDL) of proton exchange membrane (PEM) fuel cell has fibrous porous media (Tamayol and Bahrami, 2011a; Pant et al., 2012; Prasanna et al., 2004; Williams et al., 2004); a more ordered pore structure for ceramic porous materials like LSM electrode of a solid oxide fuel cell (SOFC) (Gunda et al., 2011b). For accurate pore scale studies of such applications, precise and realistic representation of such microstructural information is important for improving the efficiency of respective applications of the porous media.

With the advance in microfluidics and Micro-Electrical Mechanical System (MEMS) based microfabrication techniques, flow through miniaturized devices replicating the porous media has become an area of great interest (Bazylak

et al., 2008; Gunda et al., 2011a; Sen et al., 2012; Wan and Wilson, 1994; Wolf et al., 2008). With new and better microfabrication techniques such as LIGA (Tsakiroglou and Avraam, 2002), soft lithography(Chomsurin and Werth, 2003) and deep reactive ion etching(Berejnov et al., 2008), it is now possible to etch pores down to a few μms in width onto silicon wafers or polydimethylsiloxane (PDMS). Moving over from glass and resin based micromodels, researchers have taken advantage of microfluidic devices obtained from advanced microfabrication techniques. Perrin et al. (2006) conducted Newtonian and Non Newtonian fluid flow studies inside micro fabricated pore-network. Their micromodel consisted of 2D etched pattern of single rectangular capillaries or arrays of such capillaries in silicon. They also acknowledged the fact that the quality (accuracy and roughness) of fabrication is much better in silicon than that of the conventional glass or resin micromodels. Other works that considered pore network representation of porous media in micro fabricated models include works by Ferer et al. (2004) , Fuerstman et al. (2003) etc., which studied fluid flow in porous media.

With precise and accurate fabrication made possible by micro fabrication techniques, use of microfluidic based devices have gained immense importance in many other engineering applications too. One such class of microfluidic devices contain ordered arrangement of micro pillars that replicate fibrous porous structures. Such microporous structures offer high surface-area-to-volume ratio, enhanced heat and mass transfer coefficients and have found applications in compact heat exchangers (Kosar et al., 2005; Peles et al., 2005), microfiltration (Yoon et al., 2003), microreactors (Losey et al., 2002) and micropumping (Mathur et al., 2009). Crucial to their performance is an in-depth knowledge of pressure drop values resulting from flows inside them. Such an understanding helps in the design and optimization of these devices and better performance evaluations of such applications. Also permeability is an important property associated with any porous media that signifies the ease of fluid flow through the porous media. Permeability gives an indication of the ability of the porous media to effectively conduct fluids through them. Permeability is heavily dependent upon the interconnectedness of the pores in the medium and as such depends on the size of the solid matrix and its distribution. When only one kind of fluid is present in the porous media, the permeability is known as absolute permeability. Knowledge of permeability, as discussed previously, de-

termines the success of many enhanced oil recovery procedures. Any attempt to simulate or study the reservoir processes should need correct information of permeability.

2.4 Numerical Simulations

In addition to experimental approach, researchers have tried to understand fluid flows in porous media for calculating the various transport properties associated with the flow using numerical as well as analytical techniques. The decision for using simulation or analytical technique for solving problem depends upon various factors. For example, numerical simulations often help in getting a better picture of a complex system where analyical equations tend to add complexity. Analytical technques also include simplifying assumptions that make the problem analytically suitable though these assumptions quite often do not hold valid in practical cases. Also, numerical analysis can help in better prediction of problem solutions and results for future development which may not be possible with analytical problem solving techniques. Considering flow through porous media as complex problems due to various uncertainties involved in such flows, researchers have attempted to model these problems using different numerical simulation techniques. Monte Carlo simulation technique is one among them which have been used because of its many advantages.

Monte Carlo (MC) simulations provide a way of estimating properties using random numbers. Quite surprisingly it uses random numbers to estimate a property which is not random. These simulations help relating the data from the experimental evidences to those from the model. Monte Carlo simulations play a huge role in fluid flow simulations when there is no analytical solution available or when the pore structure geometry and fluid flow are too complex to be solved using available analytical solutions available. As discussed earlier MC simulations depend on random number generation and statistical analysis to compute the results. These simulations provide a method of converging to the realistic result using a stochastic and probabilistic approach.

Raychaudhuri (2008) in his paper on introduction to Monte Carlo Simulations, describes the Monte Carlo simulations as a what-if analysis. Developing

and employing mathematical models are a common way of solving many engineering and other scientific problems. These Mathematical models depend on certain inputs. These inputs are then processed based on a certain formulas in the model which gives rise to one or multiple outputs. Monte Carlo simulations work on the principle that these input data should be sampled from a distribution which closely resembles the real time data so as to minimize the variations in the output associated with these input data. An incorrect representation of the input data can result in a false or an unrealistic output. Even otherwise, Monte Carlo simulations allow one to systematically analyze the risks associated with different types of input. The general methodology used for Monte Carlo Simulations are as follows:

- Mathematical Model generation: This step includes identifying a suitable mathematical model and set of equations which allow us to simulate the real scenario.

- Input Data Generation(Random Data generation): The next step is to identify the input data which will set the model working and bring results. This brings to the concept of Sampling. A simple sampler produces an independent sample X every time it is called. Large Monte Carlo Simulations may spend time in churning out random variables which are Independent and identically distributed (iid) random variable.

- Processing the inputs: The input data created is then used for generating the output using the mathematical model available.

- Output Analysis and decision making: This step includes the statistical statistical analysis of the output results generated for decision making.

To summarize, Monte Carlo simulations:

- Use random numbers for scientific problem solving

- Use random numbers to solve something that is not random. To illustrate this point, let X be a random variable whose expected value is A. If we select n random variable X1, X2, X3,.Xn from a distribution, then approximately

$$A = A'_n = \frac{\sum_{i=1}^{n} X_i}{n} \tag{2.1}$$

- Use the law of large numbers which state that(carrying over from above example) A'n tends to A as n tends to infinity. Even though A'_n and X_n are random and change every time we sample them, A is not random.

- Monte Carlo simulation, in fact, are two different things. Simulation refers to the generation of random variables from a certain distribution. But Monte Carlo refers , as a whole, to the statistical analysis on the results which are obtained from applying these random variables to the mathematical models.

2.4.1 Flow through porous media: Monte Carlo Simulation approach

There have been many approaches in simulating flow through porous media. Monte Carlo simulations of flow through porous media usually involves simplifying the flow geometry and making suitable assumptions which make the computational costs easy as well as bring reliable results. Common to almost all literature is the development of a model which is assumed to be the representative of real porous media. Chan et al. (1988) considered multiphase flow in porous media and used Monte Carlo simulations to obtain the flow field. Their porous medium was made of tubes and chambers. The conductivity of the tubes represented the macroscopic permeability K and the fluid capacity of the chambers represented the macroscopic porosity. They ignored the microstructure details of the porous media and modeled the porous media solely in terms of permeability K and porosity ϕ.

Another important concept which comes into picture while using Monte Carlo simulations is the concept of Random Walks. Fishman (1996) in his book on Monte Carlo Simulations explains the concept of Random walks or Random tours. A typical example which shows the use of random tours is that of the neutron transport problem. This problem deals with the designing of a containment vessel for a nuclear reactor. The vessel is of an inner radius r and contains a shield of thickness d. The random walk simulation tries to find out the probability that a neutron with initial energy E_o will escape the shielding thickness d. A detailed explanation of the methodology can be found elsewhere (Fishman, 1996).

The above example shows that Random Walk can be used in many engineering applications especially in flow simulation in porous media. Cortis and Ghezzehei (2007) approached the flow of emulsion in porous media using a continuous time random walk technique (CTRW). They use the colloid filtration theory to model their CTRW filtration equation. Though it is not clear as to how they executed the CTRW model for simulations. Kaluarachchi et al. (1995) studied the multiphase flow in a porous medium using Monte Carlo techniques. They used the input variables as Permeability, k and the soil retention parameter α. They obtained an exponential relation between permeability and pressure using the soil retention parameter, α. The log values of permeability K and the soil retention parameter α were sampled randomly from a known distribution.

Imdakm and Sahimi (1987) used the Monte Carlo simulations to model the flow of large particles through porous media. They represented the porous media as a 2D square network. The bonds of this network are taken to be the pore throats which they assumed to be cylindrical capillary tubes. The radius R of these tubes is distributed according to Rayleigh distribution. They used the MC simulation technique to calculate the permeability of the porous medium.

The advantages of Monte Carlo techniques can be many. They are flexible and have the ability to handle empirical distributions. They are easy to be extended and can be developed for solving more complex systems. As seen above, they are particularly useful when there is no deterministic solution available for a problem and needs trial and error methods for researchers to come up with an initial idea of the outcomes. At the same time, they can be run in normal computers with very less computational costs.

2.5 Scope of the present work

Thus seen so far, representation of porous media on microfluidic devices using advanced microfabrication techniques have potential uses in many engineering applications. Though a lot of work have been done to study various flow mechanisms related to energy applications in such devices, not many studies have tried to report quantified transport properties in such microfluidic de-

vices. This work tries to quantify the transport properties in such microfluidic devices that have representation in a variety of applications from oil and gas recovery to life sciences. We make use of state-of-the-art microfabrication techniques to obtain microfluidic devices that contain precise and accurate pore networks etched in silicon instead of glass or epoxy resin. This will help in obtaining more accurate transport properties when compared to other studies that did similar work on glass or resin micromodels. In some cases where we do not have analytical results available for microfluidic transport phenomena in realistic porous media geometry such as one found in real reservoirs, we discuss numerical simulations that can be used for determining transport properties in such cases. This work basically tries to cover two type of microfludic porous media for quantifying transport properties:

- Structured porous media: which contain micro cylindrical pillars in square and staggered arrangements inside a microchannel. We conduct experiments to determine the pressure drop resulting from laminar liquid flows. This will help in improved design and optimization of such devices used in applications such as micro filtration, compact heat exchangers, micro cooling etc. We compare our results with theoretical models that are available for flows in such microfluidic porous media and report deviations if any. Detailed description on related work and major findings are discussed in chapter 3.

- Unstructured porous media: which contain pore networks etched onto silicon and contained in a microfluidic device. This pore network information has been obtained from accurate characterization of real reservoir rock core using advanced microscopy techniques and is more practical as compared to the idealistic representations of such porous media which contain either straight capillary network or randomly arranged spheres or glass beads. We determine important properties like porosity and permeability which would help in future applications that use such realistic representations of porous media for enhanced oil recovery. Since a random unstructured geometry adds complexity to the problem and due to unavailability of any analytical models for such porous networks in small length scale, we also discuss the determination of effective trans-

port properties of such unstructured porous media using Monte Carlo simulation techniques.

References

Y.M. Al-Wahaibi. First-contact-miscible and multicontact-miscible gas injection within a channeling heterogeneity system. *Energy and Fuels*, 24(3): 1813–1821, 2010.

G.I. Barenblatt, V.M. Entov, and V.M. Ryzhik. *Theory of fluid flows through natural rocks.* 1990.

L. Barta and L.G. Hepler. Kinetics and energetics of oxidation of athabasca bitumenbarta1988309. *Energy and Fuels*, 2(3):309–316, 1988.

A Bazylak, V Berejnov, B Markicevic, D Sinton, and N Djilali. Numerical and microfluidic pore networks: Towards designs for directed water transport in gdls. *Electrochimica Acta*, 53(26):7630–7637, 2008.

B. Bera, N.S.K. Gunda, S.K. Mitra, and D. Vick. Characterization of nanometer-scale porosity in reservoir carbonate rock by focused ion beam-scanning electron microscopy. *Microscopy and Microanalysis*, 18(1):171–178, 2012.

V Berejnov, N Djilali, and D Sinton. Lab-on-chip methodologies for the study of transport in porous media: Energy applications. *Lab on a Chip*, 8(5): 689–693, 2008.

M.J. Blunt. Physically-based network modeling of multiphase flow in intermediate-wet porous media. *Journal of Petroleum Science and Engineering*, 20(3-4):117–125, 1998.

M.J. Blunt. Flow in porous media-pore network models and multiphase flow. *Current Opinion in Colloid and Interface Science*, 6:197–207, 2001.

M.J. Blunt, M.D. Jackson, M. Piri, and P.H. Valvatne. Detailed physics, predictive capabilities and macroscopic consequences for pore-network models of multiphase flow. *Advances in Water Resources*, 25:1069–1089, 2002.

Orr Jr. Franklin M. Campbell, Bruce T. Flow visualization for CO_2 crude oil displacements. *Society of Petroleum Engineers journal*, 25(5):665–678, 1985.

D.Y.C. Chan, B.D. Hughes, L. Paterson, and C. Sirakoff. Simulating flow in porous media. *Physical Review A*, 38(8):4106–4120, 1988.

Koplik J. Chen, J.-d. Immiscible fluid displacement in small networks. *Journal of Colloid And Interface Science*, 108(2):304–330, 1985.

C. Chomsurin and C.J. Werth. Analysis of pore-scale nonaqueous phase liquid dissolution in etched silicon pore networks. *Water Resources Research*, 39 (9):SBH111–SBH1111, 2003.

A. Cortis and T.A. Ghezzehei. On the transport of emulsions in porous media. *Journal of Colloid and Interface Science*, 313(1):1–4, 2007.

Gedeon Dagan. Statistical theory of groundwater flow and transport: Pore to laboratory, laboratory to formation, and formation to regional scale. *Water Resources Research*, 22(9 Suppl):120–134, 1986.

R.A. Dawe. *Reservoir physics at the pore scale*. 1990.

R.V. Dharmadhikari and D.D. Kale. Flow of non-newtonian fluids through porous media. *Chemical Engineering Science*, 40(3):527–528, 1985.

McDougall S.R. Sorbie K.S. Buckley J.S. Dixit, A.B. Pore-scale modeling of wettability effects and their influence on oil recovery. *SPE Reservoir Evaluation and Engineering*, 2(1):25–36, 1999.

Blunt M.J. Dong, H. Pore-network extraction from micro-computerized-tomography images. *Physical Review E*, 80(3), 2009.

F.A.L. Dullien, F.S.Y. Lai, and I.F. MacDonald. Hydraulic continuity of residual wetting phase in porous media. *Journal of Colloid And Interface Science*, 109(1):201–218, 1986.

H.I. Ene and D. Polisevski. *Thermal flow in porous media.* 1987.

H. Fadaei, B. Scarff, and D. Sinton. Rapid microfluidics-based measurement of co 2 diffusivity in bitumen. *Energy and Fuels*, 25(10):4829–4835, 2011.

J.R. Fanchi. Oil and gas in the energy mix of the 21st century. *JPT, Journal of Petroleum Technology*, 52(12):40–46, 2000.

Fatt. The network model of porous media.1. capillary pressure characteristics. *Transactions of the American Institute of Mining and Metallurgical Engineers*, 207(7):144–159, 1956a.

Fatt. The network model of porous media.3. dynamic properties of networks with tube radius distribution. *Transactions of the American Institute of Mining and Metallurgical Engineers*, 207(7):164–181, 1956b.

Fatt. The network model of porous media.2. dynamic properties of a single size tube network. *Transactions of the American Institute of Mining and Metallurgical Engineers*, 207(7):160–163, 1956c.

M. Ferer, C. Ji, G. S. Bromhal, J. Cook, G. Ahmadi, and D. H. Smith. Crossover from capillary fingering to viscous fingering for immiscible unstable flow: Experiment and modeling. *Physical Review E - Statistical, Nonlinear, and Soft Matter Physics*, 70(1 2):016303–1–016303–7, 2004.

George S. Fishman. *Monte Carlo: Concepts, Algorithms, and Applications*. Springer, 1996.

M.J. Fuerstman, P. Deschatelets, R. Kane, A. Schwartz, P.J.A. Kenis, J.M. Deutch, and G.M. Whitesides. Solving mazes using microfluidic networks. *Langmuir*, 19(11):4714–4722, 2003.

A.T. Grogan and W.V. Pinczewski. Role of molecular diffusion processes in tertiary co//2 flooding. *JPT, Journal of Petroleum Technology*, 39(5):591–602, 1987.

N.S.K. Gunda, B. Bera, N.K. Karadimitriou, S.K. Mitra, and S.M. Hassanizadeh. Reservoir-on-a-chip (roc): A new paradigm in reservoir engineering. *Lab on a Chip*, 11(22):3785–3792, 2011a.

N.S.K. Gunda, H.-W. Choi, A. Berson, B. Kenney, K. Karan, J.G. Pharoah, and S.K. Mitra. Focused ion beam-scanning electron microscopy on solid-

oxide fuel-cell electrode: Image analysis and computing effective transport properties. *Journal of Power Sources*, 196(7):3592–3603, 2011b.

A.O. Imdakm and M. Sahimi. Transport of large particles in flow through porous media. *Physical Review A*, 36(11):5304–5309, 1987.

B.Y. Jamaloei and R. Kharrat. Analysis of pore-level phenomena of dilute surfactant flooding in the presence and absence of connate water saturation. *Journal of Porous Media*, 13(8):671–690, 2010.

J.J. Kaluarachchi, A.E. Abdin, and A. Barakat. Monte carlo analysis of two-phase (water and oil) flow in heterogeneous porous media. *Models for assessing and monitoring groundwater quality. Proc. symposium, Boulder, 1995*, 227:213–222, 1995.

A.M. Kharrat. Characterization of canadian heavy oils using sequential extraction approach. *Energy and Fuels*, 23(2):828–834, 2009.

J. Koplik and T.J. Lasseter. Two-phase flow in random network models of porous media. *Society of Petroleum Engineers journal*, 25(1):89–100, 1985.

A. Kosar, C. Mishra, and Y. Peles. Laminar flow across a bank of low aspect ratio micro pin fins. *Journal of Fluids Engineering, Transactions of the ASME*, 127(3):419–430, 2005.

C.P. Kyan, D.T. Wasan, and R.C. Kintner. Flow of single-phase fluids through fibrous beds. *Industrial and Engineering Chemistry Fundamentals*, 9(4): 596–603, 1970.

R. Lenormand and C. Zarcone. Two-phase flow experiments in a two-dimensional permeable medium. *PHYSICOCHEM. HYDRODYN.*, 6(5-6 , 1985):497–506, 1985.

R Lenormand and C Zarcone. Physics of blob displacement in a two-dimensional porous medium. *SPE Formation Evaluation*, 3(1):271–275, 1988.

M.W. Losey, S.L. Jackman, R.J.and Firebaugh, M.A. Schmidt, and K.F. Jensen. Design and fabrication of microfluidic devices for multiphase mixing and reaction. *Journal of Microelectromechanical Systems*, 11(6):709–717, 2002.

Mohanty K.K. Mani, V. Pore-level network modeling of three-phase capillary pressure and relative permeability curves. *SPE Journal*, 3(3):238–247, 1998.

D.J. Manlowe and C.J. Radke. A pore-level investigation of foam/oil interactions in porous media.

D.J. Manlowe and C.J. Radke. A pore-level investigation of foam/oil interactions in porous media. 1966.

C.M. Marle. *Multiphase flow in porous media.* 1981.

E.A. Mason, A.P. Malinauskas, and R.B. Evans III. Flow and diffusion of gases in porous media. *The Journal of Chemical Physics*, 46(8):3199–3216, 1967.

A. Mathur, S.S. Roy, M. Tweedie, S. Mukhopadhyay, S.K. Mitra, and J.A. McLaughlin. Characterisation of pmma microfluidic channels and devices fabricated by hot embossing and sealed by direct bonding. *Current Applied Physics*, 9(6):1199–1202, 2009.

C. Mattax and J. Kyte. *Oil Gas*, 59:115 –128, 1961.

Laura M. McDowell-Boyer, James R. Hunt, and Nicholas Sitar. Particle transport through porous media. *Water Resources Research*, 22(13):1901–1921, 1986.

R.J. Millington. Gas diffusion in porous media. *Science*, 130(3367):100–102, 1959.

Norman R. Morrow, Hau T. Lim, and Jill S. Ward. Effect of crude-oil-induced wettability changes on oil recovery. *SPE Formation Evaluation*, 1(1):89–103, 1986.

M. Muskat. The production histories of oil producing gas-drive reservoirs. *Journal of Applied Physics*, 16(3):147–159, 1945.

J.H. Nam and M. Kaviany. Effective diffusivity and water-saturation distribution in single- and two-layer pemfc diffusion medium. *International Journal of Heat and Mass Transfer*, 46(24):4595–4611, 2003.

H.M. Nguyen and A.M. Clarence. Videomicroscopy study of vertical flow of organic liquids in wet and dry heterogeneous porous media. *Chemical Engineering Communications*, 119(1):261–272, 1993.

Owete S. Owete and William E. Brigham. Flow behavior of foam: A porous micromodel study. *SPE Reservoir Engineering (Society of Petroleum Engineers)*, 2(3):315–323, 1987.

L.M. Pant, S.K. Mitra, and M. Secanell. Absolute permeability and knudsen diffusivity measurements in pemfc gas diffusion layers and micro porous layers. *Journal of Power Sources*, 206:153–160, 2012.

Y. Peles, A. Kosar, C. Mishra, C.-J. Kuo, and B. Schneider. Forced convective heat transfer across a pin fin micro heat sink. *International Journal of Heat and Mass Transfer*, 48(17):3615–3627, 2005.

Pinczewski W.V. Chan D.Y.C. Paterson L. ren P.E. Pereira, G.G. Pore-scale network model for drainage-dominated three-phase flow in porous media. *Transport in Porous Media*, 24(2):167–201, 1996.

C.L. Perrin, P.M.J. Tardy, K.S. Sorbie, and J.C. Crawshaw. Experimental and modeling study of newtonian and non-newtonian fluid flow in pore network micromodels. *Journal of Colloid and Interface Science*, 295(2): 542–550, 2006.

M. Prasanna, H.Y. Ha, E.A. Cho, S.-A. Hong, and I.-H. Oh. Influence of cathode gas diffusion media on the performance of the pemfcs. *Journal of Power Sources*, 131(1-2):147–154, 2004.

S. Raychaudhuri. Introduction to monte carlo simulation. In *Simulation Conference, 2008. WSC 2008. Winter*, pages 91–100. IEEE, 2008.

D. Sen, D.S. Nobes, and S.K. Mitra. Optical measurement of pore scale velocity field inside microporous media. *Microfluidics and Nanofluidics*, 12(1-4):189–200, 2012.

C.S. Simmons. A stochastic-convective transport representation of dispersion in one-dimensional porous media systems. *Water Resources Research*, 18 (4):1193–1214, 1982.

R.V. Smith and Paul D. Fleming III. Fundamental mechanisms influencing enhanced recovery of crude oil. *World Oil*, 3:291–301, 1980.

W.E. Soll, M.A. Celia, and J.L. Wilson. Micromodel studies of three-fluid porous media systems: pore-scale processes relating to capillary pressure-saturation relationships. *Water Resources Research*, 29(9):2963–2974, 1993. cited By (since 1996) 55.

H. Soo and C.J. Radke. Velocity effects in emulsion flow through porous media. *Journal of Colloid And Interface Science*, 102(2):462–476, 1984.

H. Soo and C.J. Radke. A filtration model for the flow of dilute, stable emulsions in porous media-i. theory. *Chemical Engineering Science*, 41(2):263–272, 1986.

A. Tamayol and M. Bahrami. Transverse permeability of fibrous porous media. *Physical Review E - Statistical, Nonlinear, and Soft Matter Physics*, 83(4), 2011.

D.H. Tang, E.O. Frind, and E.A. Sudicky. Contaminant transport in fractured porous media: analytical solution for a single fracture. *Water Resources Research*, 17(3):555–564, 1981.

J.J. Trivedi and T. Babadagli. Oil recovery and sequestration potential of naturally fractured reservoirs during co2 injection. *Energy and Fuels*, 23(8): 4025–4036, 2009.

C.D. Tsakiroglou and D.G. Avraam. Fabrication of a new class of porous media models for visualization studies of multiphase flow processes. *Journal of Materials Science*, 37(2):353–363, 2002.

M.I.J. Van Dijke, M. Lorentzen, M. Sohrabi, and K.S. Sorbie. Pore-scale simulation of wag floods in mixed-wet micromodels. *SPE Journal*, 15(1): 238–247, 2010.

Jiamin Wan and J.L. Wilson. Colloid transport in unsaturated porous media. *Water Resources Research*, 30(4):857–864, 1994.

H. Wen, H.M. Bambhania, and S. Calabrese Barton. Carbon nanotube-modified biocatalytic microelectrodes with multiscale porosity. *Journal of Applied Electrochemistry*, 42(3):145–151, 2012.

S. Whitaker. The equations of motion in porous media. *Chemical Engineering Science*, 21(3):291–300, 1966.

M.V. Williams, L. Begg, E.and Bonville, H.R. Kunz, and J.M. Fenton. Characterization of gas diffusion layers for pemfc. *Journal of the Electrochemical Society*, 151(8):A1173–A1180, 2004.

F.G. Wolf, L.O.E. Santos, and P.C. Philippi. Micro-hydrodynamics of immiscible displacement inside two-dimensional porous media. *Microfluidics and Nanofluidics*, 4(4):307–319, 2008.

B. Yadali Jamaloei, M. Dong, N. Mahinpey, and B.B. Maini. Enhanced cyclic solvent process (ecsp) for heavy oil and bitumen recovery in thin reservoirs. *Energy and Fuels*, 26(5):2865–2874, 2012.

Y.-K. Yoon, J.-H. Park, F. Cros, and M.G. Allen. Integrated vertical screen microfilter system using inclined su-8 structures. pages 227–230, 2003.

S. Zendehboudi, I. Chatzis, A. Shafiei, and M.B. Dusseault. Empirical modeling of gravity drainage in fractured porous media. *Energy and Fuels*, 25(3): 1229–1241, 2011.

N. Zhang and Z.N. Sun. Experimental investigation on resistance characteristics of two-phase flow through porous media channel. *Hedongli Gongcheng/Nuclear Power Engineering*, 32(3):106–110+126, 2011.

Chapter 3

Measurement of pressure drop and flow resistance in microchannels with integrated micropillars [1]

3.1 Introduction

As discussed in the previous chapter, with advances in microfluidics, flow through miniaturized devices replicating the porous media has become an area of great interest (Bazylak et al., 2008; Gunda et al., 2011a; Sen et al., 2012; Wan and Wilson, 1994; Wolf et al., 2008). With advanced microfabrication techniques such as LIGA (Tsakiroglou and Avraam, 2002), soft lithography (Chomsurin and Werth, 2003) and deep reactive ion etching (Berejnov et al., 2008), microchannels with integrated micropillars (MCIPs) have been fabricated to replicate fibrous structures in small length scales. Such microporous structures offer high surface-area-to-volume ratio, enhanced heat and mass transfer coefficients and have found applications in compact heat exchangers (Kosar et al., 2005; Peles et al., 2005), microfiltration (Yoon et al., 2003), microreactors (Losey et al., 2002) and micropumping (Mathur et al., 2009).

Traditional efforts to study fluid flow through fibrous structures have been limited to macro-scale flow that considered simplified pillar geometry and arrangement. Theoretical studies include work done by Kuwabara (1959) which

[1] A version of this chapter has been submitted for publication in *Microfluidics and Nanofluidics*, August 2012, *In review*

considers Stokes approximation for solving flow through randomly distributed parallel cylinders. Hasimoto (1959) and Ogata and Amano (2006) considered cubic array and infinite periodic array of spheres, respectively, and used Stokes equation to obtain the fluid flow solution. Numerical simulations by Firdaouss and Duplessis (2004) considered arrays of squares and rectangles to obtain solution to Stokes equation. They considered both square and staggered arrays for their simulations. Higdon (1996) presented both numerical and theoretical estimates for permeability values in porous media that consisted of ordered networks of cylinders on regular cubic lattices. van Doormaal and Pharoah (2009) conducted Lattice Boltzmann simulations to calculate the permeability in anisotropic porous gas diffusion layer(GDL) of PEM fuel cells. Their numerical model consisted of parallel and perpendicular cylindrical pillars. Jaganathan et al. (2008) carried out computational fluid dynamics(CFD) simulations to determine the permeability by processing three-dimensional (3D) image reconstructions of actual fibrous porous media. Yazdchi et al. (2011) studied the effect of microstructural properties on the macroscopic permeability of regular array of cylinders with the flow field perpendicular to the cylinder axes. They used a combination of analytical technique and finite element based numerical simulation. Tamayol et al. has performed comprehensive studies on determining transport properties of various types of fibrous porous media including metalfoams, GDLs, and arrays of cylinders (Tamayol and Bahrami, 2011b; Tamayol et al., 2012c,d).

However, studies at microscale level in fibrous structures have been limited. Also, the available studies have shown deviations from the flow mechanism predicted by macroscale models. For eg., experimental pressure drop measurements by Kosar et al. (2005) showed that the macroscale correlations do not explain the results in microscale flow. Studies by (Vanapalli et al., 2007; Yeom et al., 2009) done in the past considered micro fibrous structures but they did not take into account the effect of wall confinement in such structures. To account for small length scale and wall confinement, Tamayol et al. (2012b) performed analytical and experimental investigations of flow through such ordered packed fibrous porous materials. Their model consisted of square arrangement of pillars in polydimethylsiloxane (PDMS) microchannels over a wide range of porosity. However, the microfabrication process used in their work with PDMS as substrate material resulted in uncertainty in the geomet-

ric dimensions of the microfluidic device. This may have impact in terms of validating their theoretical models with experimental results.

Thus to overcome the existing deficiencies in producing accurate microstructures due to limitations in microfabrication processes adopted earlier by the researchers (Tamayol et al., 2012b) and to cover a wide range of porosity and pillar arrangements, we perform an extensive fluid flow study through MCIPs consisting of square and staggered arrangement of cylindrical micropillars. These MCIPs are fabricated on silicon wafers using deep reactive ion etching (DRIE) that result in smooth, vertical and precise fabrication of cylindrical micropillars. Experiments are conducted to measure the pressure drop and the resulting flow resistance across the channel for low Reynolds numbers, representing the creeping flow regime. The values of the pressure drop and the flow resistance are compared with the existing theoretical models for ordered cylinder arrangements in both macro and micro scales.

3.2 Fabrication Procedure

The silicon (Si) microchannels, consisting of micropillars, were fabricated using deep reactive ion etching microfabrication technique which is briefly described in Fig.3.1. Different models with integrated micropillars were designed in AUTOCAD (Autodesk Inc., San Rafael, CA,USA). Each model consists of a region containing micropillars arranged in either square or staggered arrangement, inlet and exit regions, and microfluidic ports. The microfluidic devices were designed in a way to cover a range of different pillar diameter and porosity. The dimensions of the fabricated samples are listed in Table 3.1 and shown in Fig.3.2. A description of the fabrication procedure of microchannel with integrated pillars is given here briefly. Details of the fabrication process can be found elsewhere (Yeom et al., 2009).

A 100-mm-diameter Si substrate (Silicon Valley Microelectronics Inc., Santa Clara, CA) was cleaned in a standard Piranha solution (H_2SO_4 and H_2O_2 in 3:1 ratio) and then dried with Nitrogen gas. A 0.5-micron oxide layer was deposited on the substrate followed by spin-coating of the positive photo resist (PPR) HPR 506 (Fuji-film Electronic Materials Inc., Mesa, Arizona). The integrated micropillars were patterned on PPR with standard photolithography

and then the oxide layer was etched with dry etching technique. This was followed by anisotropic etching of Si for about 100 μm using DRIE method. After etching, the photoresist was removed by placing the etched substrate in an acetone solution and followed by the removal of the oxide layer using buffered hydrofluoric acid (BHF).

For experimental investigation of fluid flow through microchannels, often a closed microfluidic device is preferred. The fabricated silicon microchannel with integrated micropillars is an open channel device which makes it unsuitable for the purpose of experimental investigations. To resolve this, a borofloat glass layer which consists of inlet and outlet ports drilled using abrasive waterjet cutter(2652 Jet Machining Center, OMAX, KENT,WA), is used as a cover layer for the silicon microchannel. Both the bottom layer with fabricated micropillars and the top covering layer are piranha-cleaned once again in similar composition as before (H_2SO_4 and H_2O_2 mixture in 3:1). The top layer of glass (with inlet and outlet ports) and the bottom layer of silicon containing the micropillars were anodically bonded using SUSS Bonder (CB6L, SUSS Microtec, Garching, Germany).

3.3 Experimental measurements

The experimental set up to measure pressure drop in the micropillars is shown in Fig.3.3. The set up consists of a microscope (180x magnification, 1.3M pixel CMOS image sensor, View Solutions GE-5, Howard Electronic Instruments Inc., El Dorado, KS) for the visualization of the flow through the microchannels. The inlet of the microfluidic chip was connected to a syringe pump (Harvard Apparatus, MA) which controls the flow of liquid to the test channels. The outlet was connected to a tube which was kept open to the atmosphere. For measuring the inlet pressure, a pressure transducer (0-5 PSI gauge, Omega Engineering Inc., Laval, Quebec, Canada) was used in line before the inlet port of the microchannels. The pressure was recorded by using a Data Acquisition device (DAQ) ($\pm$20 mA/$\pm$10V, 24-Bit Analog Input, National Instruments, Austin, TX). The outlet port of the microchannel was connected to a precision volumetric cylinder to collect the outlet discharge.

Appropriate tubing was selected to ensure leak proof flow connections.

The electric terminals of the pressure transducer were connected to the DAQ device which was then connected to a computer. De-ionized water was injected into the channel by the syringe pump at appropriate flow rates which were determined by the experimental constraints. The pressure at the inlet was measured by means of the pressure transducer and recorded on a computer using the DAQ device. The values of pressure drop across the micropillar region was recorded for varying flow rates. These pressure drop values are used to calculate the permeability by using Darcy's law given by:

$$K = \frac{Q \times \mu \times L}{A \times \Delta P} \tag{3.1}$$

where K is the permeability, Q is the flow rate of water, μ is the viscosity of water, L is the length of the microchannel domain consisting of micropillars, A is the flow cross sectional area and ΔP is the pressure difference between the inlet and outlet ports of the microchannel.

3.4 Theoretical Formulation for pressure drop and permeability estimation

Several models are available for calculating the permeability in fibrous structures that consist of an ordered array of cylinders. Table 3.2 provides a list of analytical models that have been used to compare the experimental results. The different analytical models provided in Table 3.2 are developed for transverse flow of fluid over an infinite number of cylinders in a row and thus neglecting the effect of channel walls on such flows. Though the majority of the models are developed for macroscopic flow, Tamayol et al. (2012b) recently developed correlations for both permeability and pressure drop in MCIPs. They considered the modified Darcy's law for laminar flow in confined porous media which was given by Brinkmann (Kaviany, 1995):

$$-\frac{dP}{dx} = \frac{\mu}{K}U + \mu^* \frac{d^2U}{dy^2} \tag{3.2}$$

where μ^* is the effective viscosity. Tamayol et al. (2012b) have reported that the viscosity ratio $\left(\mu' = \frac{\mu^*}{\mu}\right)$ for porous media consisting of arrays of cylinders can be taken as $1/\epsilon$ as suggested by Ochoa-Tapia and Whitaker (1995), where ϵ is the porosity of the medium. They obtained the expression for flow resistance by solving the Brinkman equation for small aspect ratio channels, which is

given as (Tamayol et al., 2012b):

$$\frac{\Delta P}{L\mu U} = -\frac{W \sinh\left(\frac{h}{\sqrt{\mu' K}}\right)}{K\left\{2\frac{\sqrt{\mu' K}}{h}\left[-1+\cosh\left(\frac{h}{\sqrt{\mu' K}}\right)\right]-\sinh\left(\frac{h}{\sqrt{\mu' K}}\right)\right\}} \tag{3.3}$$

where h and W are the height and width of the microchannel, respectively. The permeability K, which appears in the Eq.(3.3), has been derived by Tamayol and Bahrami (2011c) using a scaling analysis. The permeability is given as a function of porosity of the microchannels. The expressions for the porosity for square and staggered arrangement are given as (Tamayol and Bahrami, 2011a):

$$\epsilon = \begin{cases} 1-\frac{\pi d^2}{4S^2} & \text{Square} \\ 1-\frac{\pi d^2}{2\sqrt{3}S^2} & \text{Staggered} \end{cases} \tag{3.4}$$

where d is the diameter of the pillars and S is the distance between pillar centers.

Further, the expressions for the dimensionless permeability of square and staggered arrangement of pillars are (Tamayol and Bahrami, 2011a):

$$\frac{K}{d^2} = \begin{cases} \frac{0.16\left[\frac{\pi}{4\psi}-3\sqrt{\frac{\pi}{4\psi}}+3-\sqrt{\frac{4\psi}{\pi}}\right]}{\sqrt{1-\psi}} & \text{Square} \\ \frac{0.16\left[\frac{\pi}{2\sqrt{3}\psi}-3\sqrt{\frac{\pi}{2\sqrt{3}\psi}}+3-\sqrt{\frac{2\sqrt{3}\psi}{\pi}}\right]}{\sqrt{1-\psi}} & \text{Staggered} \end{cases} \tag{3.5}$$

where ψ is the solid volume fraction, which is given as 1-ϵ.

3.5 Results and Discussion

The fabricated MCIPs are characterized with optical microscope, scanning electron microscope and surface profilometer to verify the actual dimensions and roughness. Figure 3.2 shows square and staggered arrangement of pillars in MCIPs and Fig. 3.2(b) shows the optical image of one of the fabricated MCIPs. Table 3.1 provides the dimensions of the fabricated MCIPs where d is cylindrical pillars diameter, S is distance between pillars, W is the width of the microchannel, h is the depth of the channel or height of the pillar, L is the distance occupied by pillars, NSq is the notation for square arrangement and NSt is the notation for staggered arrangement. For example, the arrangement NSq 50-100 corresponds to a square configuration of pillars with a pillar diameter of 100 μm and porosity of 50%. Figure 3.4 shows the SEM images

of the fabricated MCIPs before being bonded with the glass covering layer. It is also found that the roughness of the fabricated chips is of $\sim 1 - 10$ nm. It is observed that the designed dimensions are closely matching with the fabricated dimensions and thus validating the accurate and the precise fabrication method used in this work.

Pressure drop per unit length for different flow rates of de-ionized (DI) water injected into the MCIPs is shown in Fig.3.5. These measurements are taken for all the configurations shown in Table 3.1. The total pressure drop is given by (Akbari et al., 2009):

$$\Delta P_{total} = \Delta P_{C,I} + \Delta P_{C,O} + \Delta P_D + \Delta P_{FD} + \Delta P_{minor} + \Delta P_{ev} \tag{3.6}$$

where $\Delta P_{C,I}$ is the pressure loss in the inlet tube between the pressure transducer and the inlet port of the microchannel, $\Delta P_{C,O}$ is the pressure drop in the outlet tube connected to the outlet port of the microchannel, ΔP_D is the pressure drop in the entrance region where the flow is still not fully developed, ΔP_{FD} is the pressure drop in the fully developed region of the MCIP, ΔP_{minor} is the pressure drop due to the 90° bends at the inlet and the outlet ports and due to the sudden expansion and contraction at the inlet and outlet ports respectively, and ΔP_{ev} is the pressure drop due to electroviscous effect. For detailed calculation of these individual pressure drops, readers can refer to the information provided in the appendix.

It is found that the pressure drop follows a linearly increasing trend with increasing flow rates for both square and staggered arrangement in MCIPs as shown in Fig.3.5. In both the arrangements, the MCIP with the least porosity produces the largest pressure drop thus signifying higher flow resistance in a given MCIP. Figure 3.5(a) shows the pressure drop trend for different flow rates in MCIPs with square arrangement along with the error bars associated with the measurements. For detailed calculation of the error estimates, readers can refer to the supplementary information provided by the authors. NSq 50-100, which has the maximum pillar diameter and the least porosity, develops largest pressure drop for different injection rates. It can be seen that the pressure drop for NSq 90-30 is greater than that for NSq 80-50 for higher flow rates which is counter intuitive. As the porosity increases in MCIPs, the slope of the pressure drop line decreases thus showing less resistance to flow

rates in such MCIPs. Figure 3.5(b) shows the variation of pressure drop for different flow rates in MCIPs with staggered arrangement. As observed in the square arrangement, pressure drop in staggered arrangement also decreases with increasing porosity. In general, for the same pillar diameter and porosity, MCIPs with square arrangement gives higher pressure drop when compared to their counterparts for any given flow rate.

Figure 3.6 shows the variation of experimental flow resistance, $\Delta P/Q$, with varying Darcy number for different MCIPs with square and staggered arrangements and their comparison with the analytical model developed by Tamayol et al. (2012b) as given in Eq.(3.3). Here Darcy number is defined as $\sqrt{K/h^2}$, where K is the theoretical permeability predicted by Eq. (3.5) and h is the height of the microchannel. For both the pillar arrangements, the flow resistance decreases as the Darcy number increases. Figure 3.6(a) shows the experimental flow resistance in MCIPs for square arrangement and its comparison with the analytical model. The experimentally obtained $\Delta P/Q$ values vary between $\pm 9\%$ of the values reported. It can be seen that the deviations from the theoretical results are maximum at low Darcy numbers which decreases as the Darcy number increases. This is also true for MCIPs with staggered arrangement, which is evident from Fig.3.6(b). In case of staggered arrangement, $\Delta P/Q$ is maximum for the chip that has the lowest Darcy number. This trend is also predicted by the theoretical model but there are still deviations between the experimental and theoretical values of flow resistance. For the same Darcy number, the square arrangement gives higher value of $\Delta P/Q$ compared to the staggered arrangement of pillars.

The variation of experimental $\Delta P/L\mu U$, with flow rate for different MCIPs and its comparison with theoretical model, as provided in Eq.(3.3), is shown in Fig.3.7. $\Delta P/L\mu U$ can be taken as another indicator of the flow resistance offered by the MCIPs. It is observed that, the MCIPs with larger pillar diameter and hence low porosity offers higher flow resistance in both square and staggered arrangements. The experimental values of $\Delta P/L\mu U$ for different MCIPs in both the arrangements almost remain constant with some deviations. The errors in the reported values range between $\pm 9\%$. These deviations are more prominent in MCIPs with larger pillar diameter. The experimentally obtained flow resistance values are compared with the theoretical model. The differences

between the experiment and the theoretical values are prominent in MCIPs with larger pillar diameter. In general, the MCIPs with square arrangement offers higher resistance to flow than their staggered counterparts.

Figure 3.8 shows the comparison of the experimentally derived permeability values, with those given by different analytical models listed in Table 3.2. Figure 3.8(a) shows the comparison of the experimentally obtained permeability values for square arrangement to the theoretical permeability values from existing macroscale and microscale models. It is evident that none of the existing models can predict the experimental trend for the porosity range used here. Figure3.8(b) shows similar comparisons for MCIPs with staggered arrangement of micropillars. As observed here, the existing models fail to predict the permeability values obtained from experimental measurements in MCIPs. The microscale permeability model given by Eq.(3.5) also fails to accurately predict the trend though the deviations are less as the porosity decreases. These experimental results points to the fact that when finite wall effects are present along with accurately obtained microfabricated features in MCIP, the existing theoretical models for predicting permeability need to be re-visited and most probably need to be altered to accurately capture the flow conditions in such microfluidic devices.

For further investigating the effect of micro-pillar arrangement on the flow resistance of the MCIP, a typical channel with a constant width of 2 mm and depth of 100 μm is considered here. Moreover, two micropillar sets with diameters of 10 μm and 50 μm are considered for the investigation (Tamayol et al., 2012a). As can be seen from Fig. 3.9, there is an inverse relationship between the porosity and the flow resistance. At a constant porosity (the same surface-to-volume ratio), channel with square arrangement offers higher flow resistance when compared to its staggered counterpart. This difference is more pronounced in lower porosities where the difference between permeability values calculated by Eq.(3.5) is more significant. The results also suggest that, at any constant porosity, a channel with pillars of smaller diameter offers higher flow resistance.

3.6 Conclusion

Pressure drop and flow resistance for single phase flow through microchannels with integrated micropillars (MCIPs) were experimentally determined. For this purpose, different silicon microchannels were fabricated with integrated micropillars using deep reacting ion etching (DRIE) technique. The pillars were arranged in square and staggered pattern in the channel and the Darcy number ranged between 0.05 and 0.31. The pressure drop values were measured experimentally to determine the flow resistance offered by different MCIPs. It is observed that the pressure drop varies linearly in all MCIPs with increasing flow rate. Flow resistance obtained from the pressure drop values was maximum for the MCIP with the minimum Darcy number. It is found that the square arrangement offers higher resistance to fluid flow when compared to their staggered counterparts. Permeabilities for the MCIPs were also calculated from the experimental pressure drop values. It is found that the experimentally obtained permeability values differ from those obtained from the existing theoretical models. Therefore, it can be concluded that the present theoretical models fail to accurate represent the permeabilities of structured porous media, such as the microchannel with integrated pillars.

Table 3.1 – Geometrical dimensions of different fabricated MCIPs considered in the present work.

Arrangement	Pillar dimensions		Channel dimensions		
	d (μm)	$S(\mu m)$	$h(\mu m)$	L(mm)	$W(\mu m)$
NSq 95-30	30	118	98.4	46.23	1190
NSq 90-30	30.42	84	98.4	37.13	841
NSq 80-50	50.23	100	98.4	34.45	990
NSq 70-50	50.2	87	98.4	24.46	808
NSq 50-100	100	127	98.4	18.87	1250
NSt 90-30	30.21	90.3	98.4	37.72	900
NSt 80-50	50	108	98.4	33.05	1064
NSt 70-50	50	87.2	98.4	24.26	869
NSt 50-100	100	135	98.4	20.11	1346

Table 3.2 – Existing analytical models for computing permeability of fibrous porous structures under transverse flows. Here d is the diameter of the pillar and ϵ is the porosity.

Author	Models for permeability (K)
Hasimoto (1959)	$\frac{d^2}{32(1-\epsilon)}\Big[-ln(1-\epsilon)-1.476\Big]$
Happel (1959)	$\frac{d^2}{32(1-\epsilon)}\Big[-ln(1-\epsilon)+\frac{(1-\epsilon)^2-1}{(1-\epsilon)^2+1}\Big]$
Kuwabara (1959)	$\frac{d^2}{32(1-\epsilon)}\Big[-ln(1-\epsilon)-1.5+2(1-\epsilon)\Big]$
Sangani and Acrivos (1982)	$\frac{d^2}{32(1-\epsilon)}\Big[-ln(1-\epsilon)-1.476$ $+2(1-\epsilon)-1.774(1-\epsilon)^2+4.076(1-\epsilon)^3\Big]$
Drummond and Tahir (1984)	$\frac{d^2}{32(1-\epsilon)}\Big[-ln(1-\epsilon)-1.473+\frac{2(1-\epsilon)-0.796(1-\epsilon)^2}{1+0.489(1-\epsilon)-1.605(1-\epsilon)^2}\Big]$
Tomadakis and Sotirchos (1993)	$\frac{d^2\epsilon}{8(ln\epsilon)^2}\Big[\frac{(\epsilon-0.33)^{2.707}}{0.67^{0.707}[1.707\epsilon-0.33]^2}\Big]$
Kaviany (1995)	$\frac{0.0606\pi d^2\epsilon^{5.1}}{4(1-\epsilon)}$
Van Der Westhuizen and Du Plessis (1996)	$\frac{\pi d^2\epsilon(1-\sqrt{1-\epsilon})^2}{96(1-\epsilon)^{1.5}}$

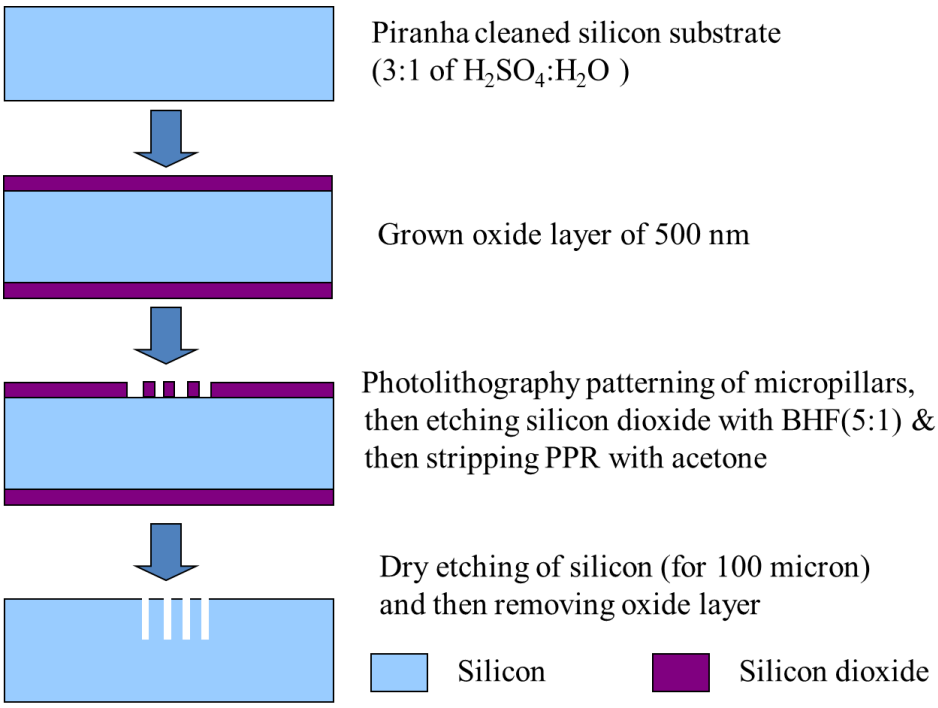

Figure 3.1 – The process flow diagram of the microfabrication technique used to generate pillars for the MCIP.

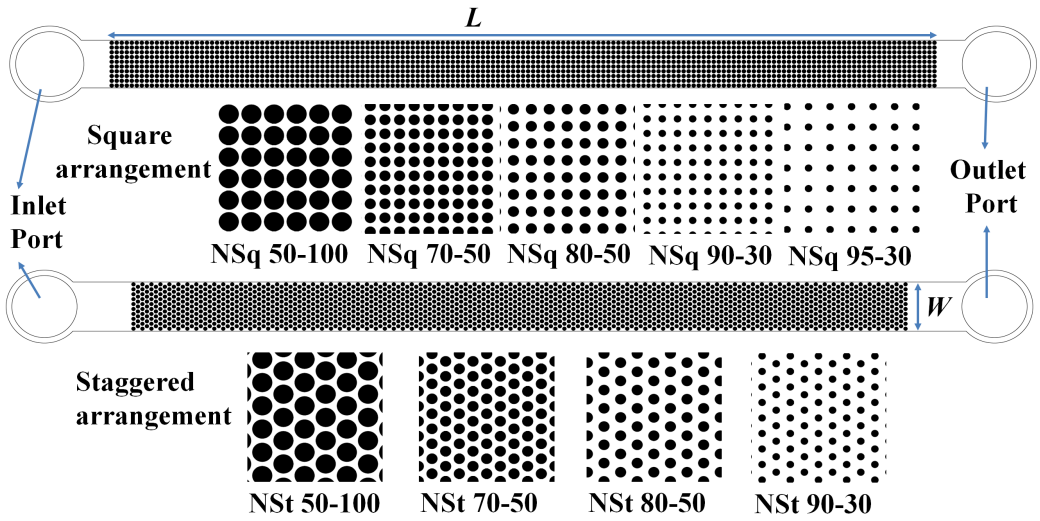

(a)

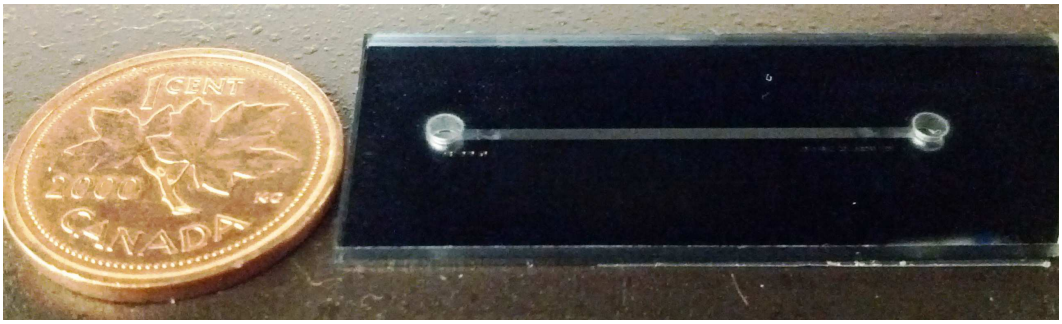

(b)

Figure 3.2 – (a)Microchannel with integrated micropillars (MCIP) considered in this work. NSq refers to square arrangement and NSt refers to staggered arrangement ; (b) Optical image of one of the fabricated MCIPs.

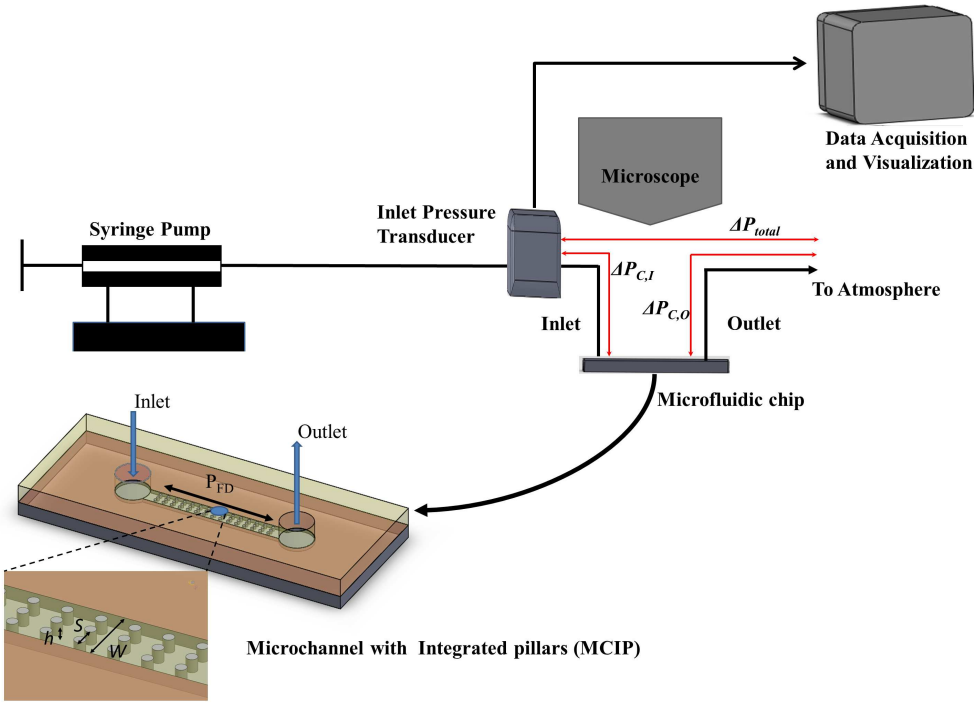

Figure 3.3 – Schematic of the experimental set-up considered for pressure drop measurements in MCIP.

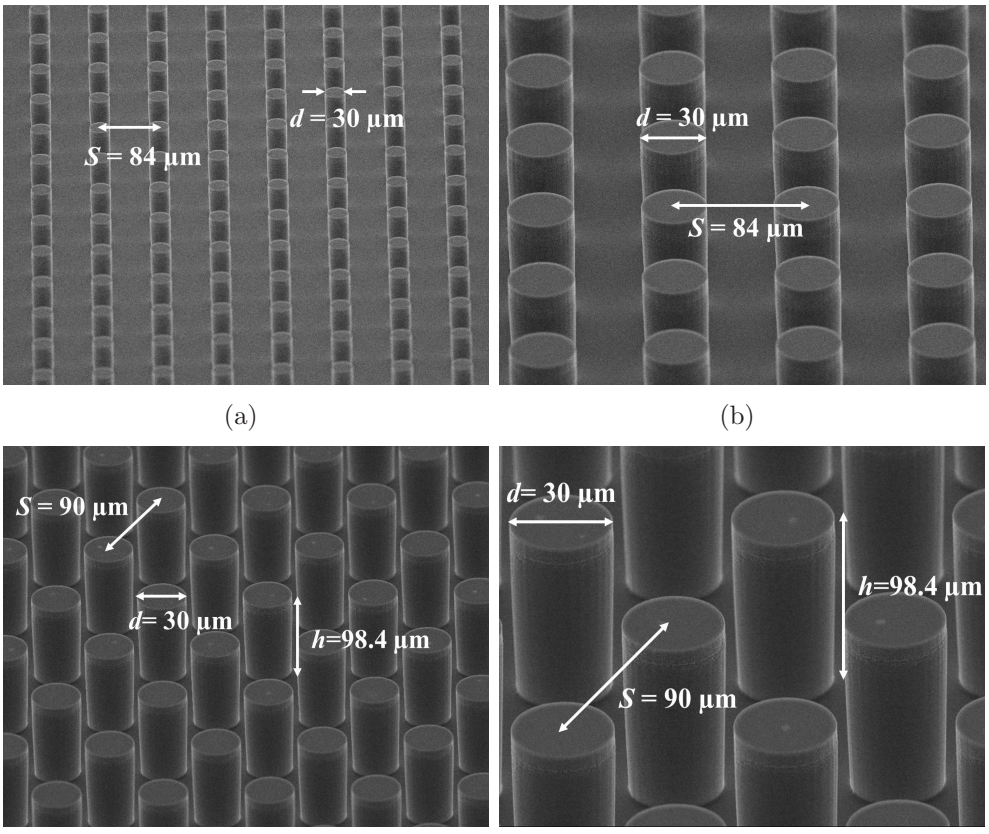

Figure 3.4 – SEM image of micropillars; (a) square arrangement; (b) magnified image of square arrangement; (c) staggered arrangement; (d) magnified image of staggered arrangement.

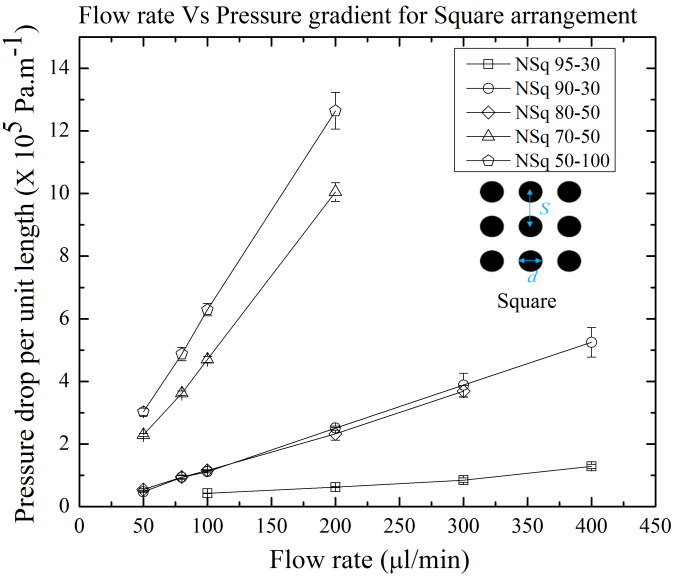

(a)

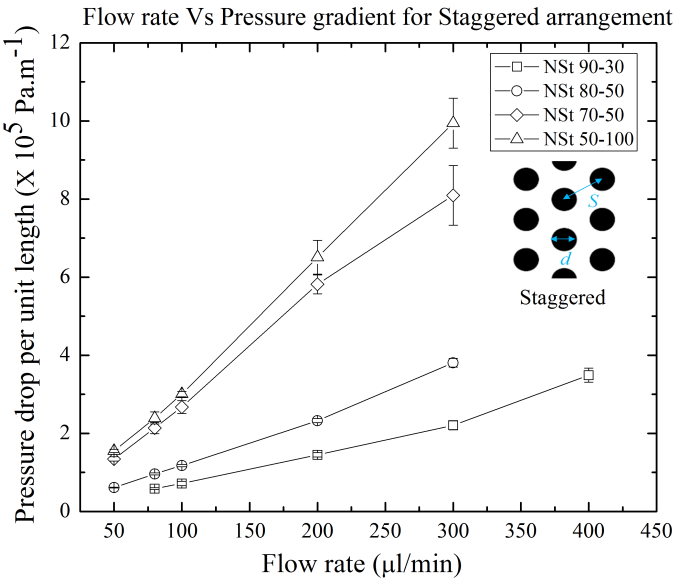

(b)

Figure 3.5 – Variation of pressure drop with change in flow rate for different arrangements of pillars; (a)square arrangement and (b)staggered arrangement.

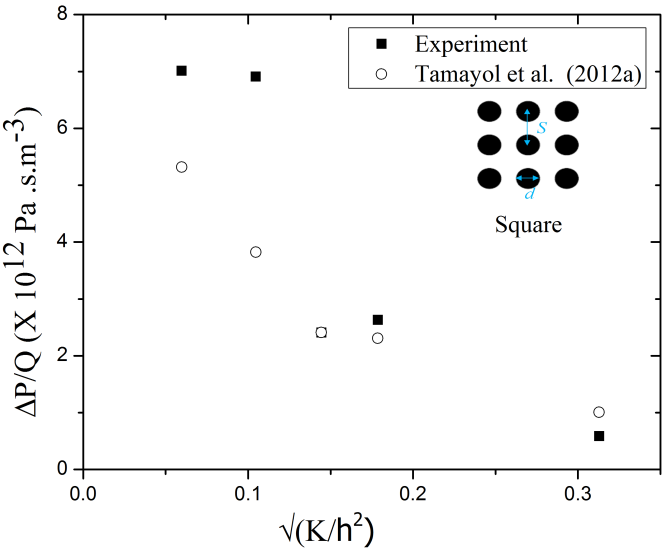

(a)

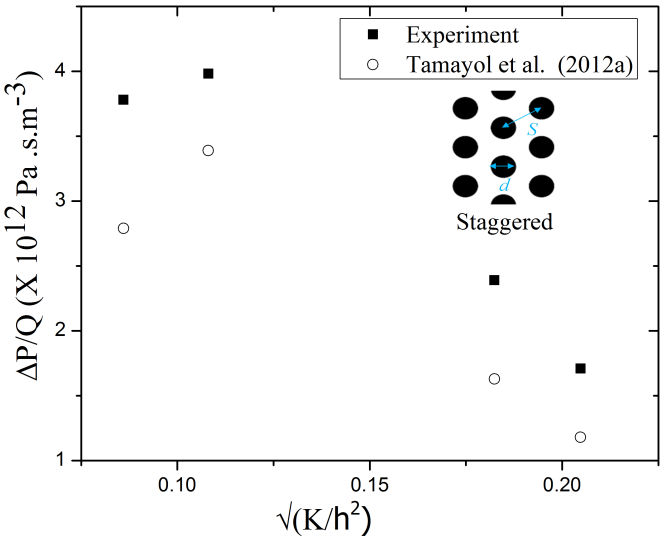

(b)

Figure 3.6 – Variation of pressure drop per unit flow rate with change in Darcy number for;(a)square arrangement and (b)staggered arrangement.

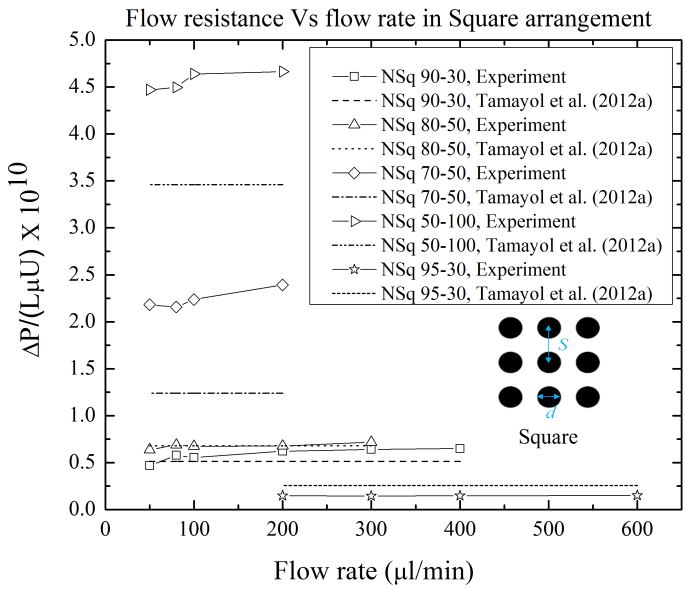

(a)

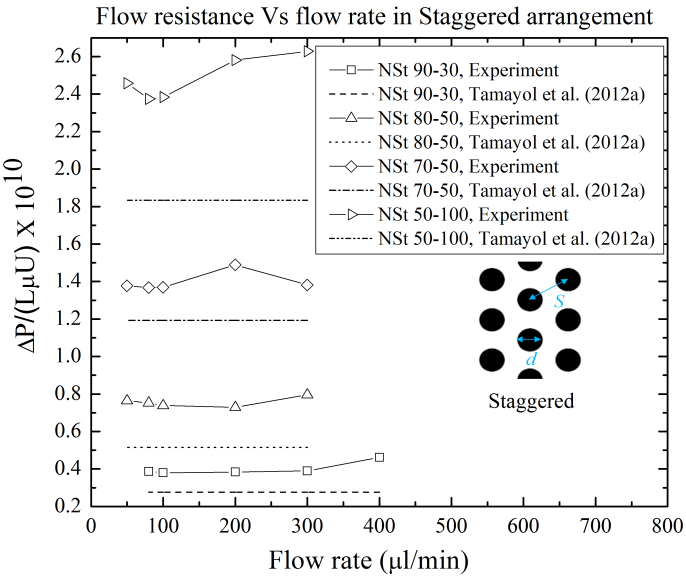

(b)

Figure 3.7 – Variation of flow resistance with change in flow rate for different arrangements; (a)square arrangement and (b)staggered arrangement.

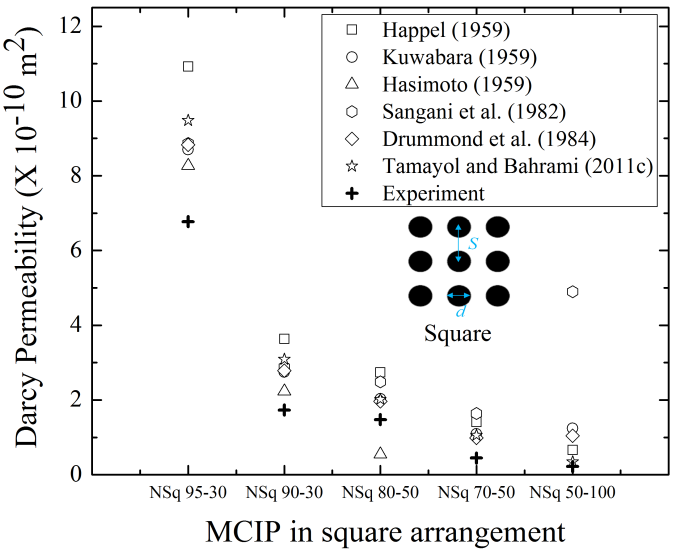

(a)

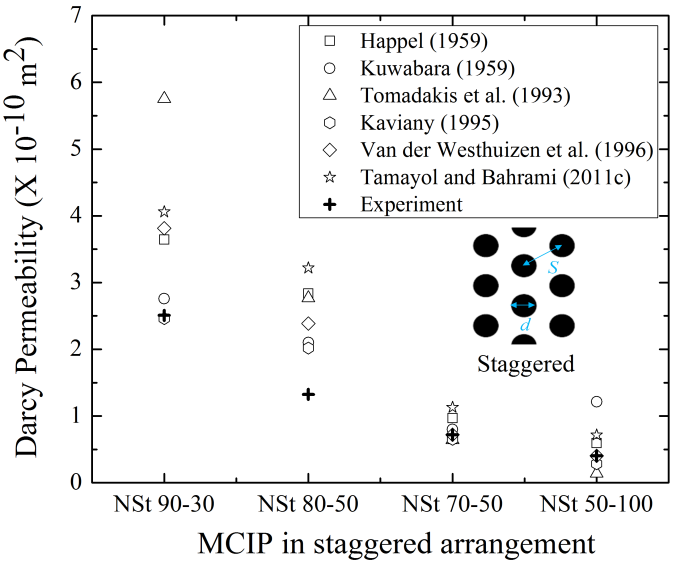

(b)

Figure 3.8 – Comparison of experimental permeability values with different existing models for MCIPs with; (a)square arrangement and (b)staggered arrangement.

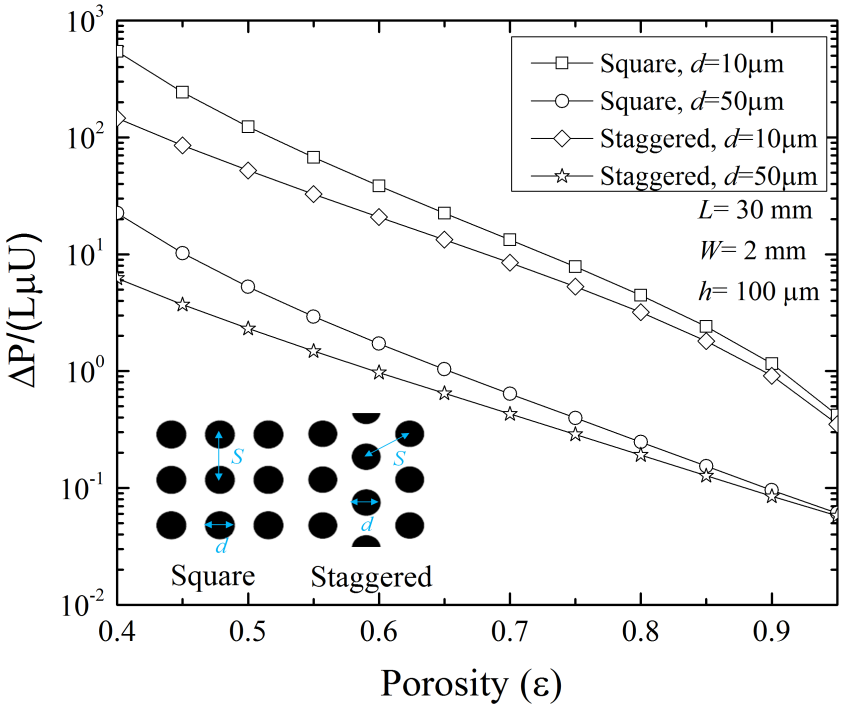

Figure 3.9 – Variation of the theoretical flow resistance (as predicted by Tamayol et al. (2012a)) with the porosity of the MCIP for square and staggered arrangements.

References

M. Akbari, D. Sinton, and M. Bahrami. Pressure drop in rectangular microchannels as compared with theory based on arbitrary cross section. *Journal of Fluids Engineering, Transactions of the ASME*, 131(4):0412021–0412028, 2009.

A Bazylak, V Berejnov, B Markicevic, D Sinton, and N Djilali. Numerical and microfluidic pore networks: Towards designs for directed water transport in gdls. *Electrochimica Acta*, 53(26):7630–7637, 2008.

V Berejnov, N Djilali, and D Sinton. Lab-on-chip methodologies for the study of transport in porous media: Energy applications. *Lab on a Chip*, 8(5): 689–693, 2008.

C. Chomsurin and C.J. Werth. Analysis of pore-scale nonaqueous phase liquid dissolution in etched silicon pore networks. *Water Resources Research*, 39 (9):SBH111–SBH1111, 2003.

J.E. Drummond and M.I. Tahir. Laminar viscous flow through regular arrays of parallel solid cylinders. *International Journal of Multiphase Flow*, 10(5): 515–540, 1984.

M. Firdaouss and J.P. Duplessis. On the prediction of darcy permeability in nonisotropic periodic two-dimensional porous media. *Journal of Porous Media*, 7(2):119–131, 2004.

N.S.K. Gunda, B. Bera, N.K. Karadimitriou, S.K. Mitra, and S.M. Hassanizadeh. Reservoir-on-a-chip (roc): A new paradigm in reservoir engineering. *Lab on a Chip*, 11(22):3785–3792, 2011.

J Happel. Viscous flow relative to arrays of cylinders. *AIChE Journal*, 5(2): 174–177, 1959.

H. Hasimoto. On the periodic fundamental solutions of the stokes equations and their application to viscous flow past a cubic array of spheres. *J. Fluid Mech*, 5(2):317–328, 1959.

Ford G.D. Higdon, J.J.L. Permeability of three-dimensional models of fibrous porous media. *Journal of Fluid Mechanics*, 308:341–361, 1996.

S. Jaganathan, H. Vahedi Tafreshi, and B. Pourdeyhimi. A realistic approach for modeling permeability of fibrous media: 3-d imaging coupled with cfd simulation. *Chemical Engineering Science*, 63(1):244–252, 2008.

M. Kaviany. *Principles of Heat Transfer in Porous Media*. Springer-Verlag, 2 edition, 1995.

A. Kosar, C. Mishra, and Y. Peles. Laminar flow across a bank of low aspect ratio micro pin fins. *Journal of Fluids Engineering, Transactions of the ASME*, 127(3):419–430, 2005.

S. Kuwabara. The forces experienced by randomly distributed parallel circular cylinders or spheres in a viscous flow at small reynolds numbers. *Journal of the Physical Society of Japan*, 14(4):527–532, 1959.

M.W. Losey, S.L. Jackman, R.J.and Firebaugh, M.A. Schmidt, and K.F. Jensen. Design and fabrication of microfluidic devices for multiphase mixing and reaction. *Journal of Microelectromechanical Systems*, 11(6):709–717, 2002.

A. Mathur, S.S. Roy, M. Tweedie, S. Mukhopadhyay, S.K. Mitra, and J.A. McLaughlin. Characterisation of pmma microfluidic channels and devices fabricated by hot embossing and sealed by direct bonding. *Current Applied Physics*, 9(6):1199–1202, 2009.

J.A. Ochoa-Tapia and S. Whitaker. Momentum transfer at the boundary between a porous medium and a homogeneous fluid-i. theoretical development. *International Journal of Heat and Mass Transfer*, 38(14):2635–2646, 1995.

H. Ogata and K. Amano. A fundamental solution method for three-dimensional viscous flow problems with obstacles in a periodic array. *Journal of Computational and Applied Mathematics*, 193(1):302–318, 2006.

Y. Peles, A. Kosar, C. Mishra, C.-J. Kuo, and B. Schneider. Forced convective heat transfer across a pin fin micro heat sink. *International Journal of Heat and Mass Transfer*, 48(17):3615–3627, 2005.

A.S. Sangani and A. Acrivos. Slow flow past periodic arrays of cylinders with application to heat transfer. *International Journal of Multiphase Flow*, 8 (3):193–206, 1982.

D. Sen, D.S. Nobes, and S.K. Mitra. Optical measurement of pore scale velocity field inside microporous media. *Microfluidics and Nanofluidics*, 12(1-4):189–200, 2012.

A. Tamayol and M. Bahrami. Transverse permeability of fibrous porous media. *Physical Review E - Statistical, Nonlinear, and Soft Matter Physics*, 83(4), 2011a.

A. Tamayol and M. Bahrami. In-plane gas permeability of proton exchange membrane fuel cell gas diffusion layers. *Journal of Power Sources*, 196(7): 3559–3564, 2011b.

A. Tamayol and M. Bahrami. Water permeation through gas diffusion layers of proton exchange membrane fuel cells. *Journal of Power Sources*, 196(15): 6356–6361, 2011c.

A Tamayol, S K Gunda, N, M Akbari, K Mitra, S, and M Bahrami. Creeping flow through microchannels with integrated micro-pillars. In *Proceedings of the ASME2012 10th International Conference on Nanochannels, Microchannels, and Minichannels, ICNMM2012 July 8-12, 2012, Puerto Rico, USA*, 2012a.

A. Tamayol, A. Khosla, B.L. Gray, and M. Bahrami. Creeping flow through ordered arrays of micro-cylinders embedded in a rectangular minichannel. *International Journal of Heat and Mass Transfer*, 55(15-16):3900–3908, 2012b.

A. Tamayol, F. McGregor, and M. Bahrami. Single phase through-plane permeability of carbon paper gas diffusion layers. *Journal of Power Sources*, 204:94–99, 2012c.

A. Tamayol, K.W. Wong, and M. Bahrami. Effects of microstructure on flow properties of fibrous porous media at moderate reynolds number. *Physical Review E - Statistical, Nonlinear, and Soft Matter Physics*, 85(2), 2012d.

M.M. Tomadakis and S.V. Sotirchos. Transport properties of random arrays of freely overlapping cylinders with various orientation distributions. *The Journal of Chemical Physics*, 98(1):616–626, 1993.

C.D. Tsakiroglou and D.G. Avraam. Fabrication of a new class of porous media models for visualization studies of multiphase flow processes. *Journal of Materials Science*, 37(2):353–363, 2002.

J. Van Der Westhuizen and J.P. Du Plessis. An attempt to quantify fibre bed permeability utilizing the phase average navier-stokes equation. *Composites Part A: Applied Science and Manufacturing*, 27(4 PART A):263–269, 1996.

M.A. van Doormaal and J.G. Pharoah. Determination of permeability in fibrous porous media using the lattice boltzmann method with application to pem fuel cells. *International Journal for Numerical Methods in Fluids*, 59(1):75–89, 2009.

S. Vanapalli, H.J.M. Ter Brake, H.V. Jansen, J.F. Burger, H.J. Holland, T.T. Veenstra, and M.C. Elwenspoek. Pressure drop of laminar gas flows in a microchannel containing various pillar matrices. *Journal of Micromechanics and Microengineering*, 17(7):1381–1386, 2007.

Jiamin Wan and J.L. Wilson. Colloid transport in unsaturated porous media. *Water Resources Research*, 30(4):857–864, 1994.

F.G. Wolf, L.O.E. Santos, and P.C. Philippi. Micro-hydrodynamics of immiscible displacement inside two-dimensional porous media. *Microfluidics and Nanofluidics*, 4(4):307–319, 2008.

K. Yazdchi, S. Srivastava, and S. Luding. Microstructural effects on the permeability of periodic fibrous porous media. *International Journal of Multiphase Flow*, 37(8):956–966, 2011.

J. Yeom, D.D. Agonafer, J.-H. Han, and M.A. Shannon. Low reynolds number flow across an array of cylindrical microposts in a microchannel and figure-of-merit analysis of micropost-filled microreactors. *Journal of Micromechanics and Microengineering*, 19(6), 2009.

Y.-K. Yoon, J.-H. Park, F. Cros, and M.G. Allen. Integrated vertical screen microfilter system using inclined su-8 structures. pages 227–230, 2003.

Chapter 4

Numerical and experimental investigations of flow through porous media at small length scales

4.1 Introduction

The previous chapter discussed about the fluid flow experiments conducted in microfluidic devices containing structured porous media. Though such devices are being used in many engineering applications as discussed in the previous chapter, not all applications that include flow through porous media contain such structured arrangements. Infact, majority of practical applications that include flow through porous media contain a random arrangement of pores and throats which renders an unstructured geometry to such porous media. Thus it becomes important to consider the unstructured geometry that is found in porous media such as reservoir rocks and fuel cell electrodes to properly account for actual porous media flow mechanism. Since microfluidic based models have been used to represent porous media, it becomes equally important that such unstructured geometry be represented on such microfluidic models for taking into account the pore scale flow mechanisms in such porous media.

As discussed in chapter 2, researchers have tried to represent realistic porous media geometry in the past in both numerical and experimental investigations. Due to the complexity involved in numerical investigations and fabrication constraints to create realistic pore geometry, previous studies could

only incorporate porous media geometry that were close approximations to the actual porous media geometry. Results of fluid flow studies obtained from such porous media representations lacked validity in terms of their proximity to realisitic phenomena. Also, approximations of the porous media geometry also meant that the inherent randomness associated with actual porous media geometry were not taken into account. This was a big deviation from the actual case which involves randomness associated with both the porous media geometry as well as the motion of fluid particles that undergo motion in such geometries as in the case of gas flows.

Thus it is important to conduct studies, both numerical and theoretical, that accounts for the actual porous media geometry in the commonly found unstructured porous media. This chapter deals with numerical as well as expermental studies of fluid flow that takes into account the realistic porous media geometry found in common applications. We first describe the numerical study done for determining effective transport properties in a porous media that is found in common applications. Simulation methods such as Monte Carlo (MC) have been used to characterize the randomness associated with such media. Most of the simulations in the past studies have been carried out in artificially generated porous media represented as random pack of spheres or randomly arranged cylindrical fibers. In our study, we apply MC simulation to images of an actual porous medium, obtained by using Focus Ion Beam Scanning Electron Microscopy (FIB SEM). This work also addresses the effect of tessellation of solid surfaces in discrete geometries on the calculation of effective transport properties. This is followed by an experimental investigation of the fluid flows in microfluidic porous media that contain pore networks of naturally found oil reservoir rocks.

4.2 Monte Carlo Simulations[1]

Computer simulations have been developed and used in the past to understand the mechanism of fluid transport through porous media (Frenkel and Smit, 1996; Landau and Binder, 2005). With the advance in computer technology, a variety of simulation techniques have been used to study the flow

[1] A version of this section has been published in the *Proceedings of the 10th International Conference on Nanochannels, Microchannels and Minichannels ICNMM 2012, July 8-12, 2012, Puerto Rico, USA*

of fluids through porous media. Some of the commonly used techniques include Molecular Dynamics (MD) and Lattice Boltzmann (LBM) simulations (Hatiboglu and Babadagli, 2007; van Doormaal and Pharoah, 2009). Both MD and LBM simulations require a lot of computational effort in terms of simulating such transport phenomena in porous media. Also, in the past all the simulations have been performed in artificially constructed porous media which are assumed to closely resemble the actual porous media. Random fibers (Sahimi and Stauffer, 1991; Tomadakis and Sotirchos, 1993; van Doormaal and Pharoah, 2009) random pack of spheres (Berson et al., 2011; Cancelliere et al., 1990) etc. have been used as examples of porous media for simulating transport processes in them. Though the solutions obtained by such simulations in artificial porous media give an approximation of the processes that occur in such media, developing or using techniques to simulate transport processes in real images of porous media will help to understand such processes much better.

In this work we use a Focused Ion Beam Scanning electron microscopy image (FIB SEM) of the porous electrode of Solid Oxide Fuel Cell (SOFC) as the porous media. The effective gas diffusivity is calculated by means of Mean Square Displacement random walk Monte Carlo (MC) method. The MC simulations have been extensively used in the past for studying the transport processes through porous media (Jain et al., 2003; Landau and Binder, 2005; Sahimi and Stauffer, 1991). The mean square displacement method for calculating the effective diffusivity has been introduced previously and has been found to be reliable for calculating effective transport properties of porous media (Sahimi and Stauffer, 1991). Berson et al. Berson et al. (2011) recently applied the mean square displacement method for calculating the effective gas diffusivity values of the SOFC porous electrode by approximating the media as a random pack of spheres. Our work focuses on calculating the effective transport properties of porous media by using realistic porous media geometry. This work includes simulating the random walk of gas particles and the consequent calculation of mean square displacement to calculate the effective diffusivity. The numerical code for the particle movement and diffusion calculation is written in MATLAB by reading a 2D FIB SEM image. This work also tries to address the problem of tessellated geometry in performing such particle movement simulations.

4.2.1 Theory

Flow of gases through the porous electrode in a SOFC electrode is mainly dominated by diffusion. The diffusivity of a gas in a porous medium is less than the actual diffusivity due to the presence of solid matrix and hence only a small amount of pore space is available for the actual flow. Calculation of effective properties gives an estimation of the actual transport properties in porous media. Diffusion in an SOFC electrode takes place through confined nano pores and hence the diffusion regime is characterized by the Knudsen number which is given as:

$$Kn = \frac{\lambda}{l} \tag{4.1}$$

Where λ is the mean free path of the gas particles and l is the characteristic length of the pore domain.
Based on the Knudsen number, the diffusion regimes can either be bulk ($Kn < 10 - 3$), transition ($0.1 < Kn < 10$) or Knudsen regime ($Kn > 10$). At any temperature, the gas particles posses thermal energy and undergo Brownian motion which is characterized by random movement of particles. In Knudsen diffusion regime, the mean free path of the particles is comparable with the characteristic length of the pore domain. In such diffusion regimes, the diffusion is dominated by the particle-wall collision rather than particle-particle interaction. From the kinetic theory of gases, the average velocity of gas molecules is given by(Kennard, 1938):

$$< \nu >= \sqrt{\frac{8k_BT}{\pi m}} \tag{4.2}$$

Where $< \nu >$ is the average velocity associated with the gas particles, k_B is the Boltzmann constant, T is the temperature of the gas and m is the mass of a single gas particle.
The effective diffusion coefficient is calculated by means of MC simulations. Brownian motion of the gas particles is simulated by random walk technique and the diffusivity calculated by the mean square displacement method. The effective diffusion coefficient D_eff is given by (Chandrasekhar, 1943; Einstein, 1956):

$$D_{eff} = \sqrt{\frac{< \eta^2 >}{6t}} \tag{4.3}$$

Where $< \eta^2 >$ is the mean square displacement and t is the time taken by the gas particles to undergo certain length of displacement.
The expression for the ratio of the effective diffusivity (D_eff) to the true diffusivity of the gas (D_o) has been given by Bruggeman (1935) as:

$$\frac{D_e}{D_o} = \epsilon^{1.5} \tag{4.4}$$

Where D_e is the effective diffusivity, D_o is the diffusivity of the gas in a medium if the medium was not porous and ϵ is the porosity. The above equation, known as Bruggeman equation, has been shown experimentally to be valid for any medium with porosity greater than 0.6.

4.2.2 Procedure

FIB-SEM, a destructive imaging technique, is used to get high resolution images of the SOFC electrode. Fig. 4.1 shows a 2D image of the SOFC electrode cross section taken with the help of SEM technique. Gunda et al. (2011b) ,in their paper, have described the procedure of obtaining such high resolution 2D images. The black region represents the solid matrix and the white region represents the pore space. The image was imported to MATLAB and was read to store the pore space and solid matrix property values. The image was discretized into 434483 pixels and each pixel was found to be of 10 nm resolution.
The porosity of the 2D image was calculated by using hit and miss Monte Carlo technique. A set of 10000 random points where located in the image and evaluated to determine if they belonged to the pore space or to the solid matrix. The fraction of the points lying in the pore space gave the value of porosity and was found to be 0.56.

The gas to be simulated was taken as Argon at room temperature. A set of simulations were carried on with the number of particles ranging from 1000 to 2000. For every particle, a random pore space was chosen in the domain and the particle was moved in that pore space. If the sample region chosen belonged to the solid matrix, a different region was chosen again to locate a position in the pore space. Figure 4.2(a) shows a sample region comprising of solid matrix and pore space. Once the particle was put in the pore space, it was moved along the pixels. Figure 4.2(b) shows a schematic of the movement of a particle

in the pore space. The length that the particle travels is varied from 1 to 20 pixels thus changing the total time required to complete the simulation. With the length of the moves increasing, the particle covers a greater area of the domain. The direction of the movement was determined by a random number generated using the random number generator in MATLAB. The particle can only move along the pixels in either right, left, up or down directions. Care was taken not to move the particle in opposite directions in subsequent steps by influencing the random number generator accordingly. Collisions with the wall were taken care of by reversing the normal velocity vector. Hence the particle bounces back once it collides with the wall. The same rule of collision was applied if the particle met any of the four boundaries of the image. The final position of the particle was stored after the total number of time steps. The effective diffusivity was then calculated by means of the mean square displacement method. The whole procedure is shown in a flowchart which can be found in the appendix section.

4.2.3 Results

The effective diffusivity was calculated in the Knudsen regime as the mean free path of the Argon gas molecules was comparable with the characteristic length of the pore domain. The characteristic length was calculated for a 2D image by using the equation below:

$$< l >= 4\frac{A}{P} \tag{4.5}$$

Where $< l >$ is the characteristic length of the pore domain, A is the area of the pore space and P is its perimeter. Both these quantities were calculated by analyzing the image showed in Fig 1 in MATLAB.

The effective diffusivity for argon calculated by random walk MC simulation in this work was found to be $1.4 \times 10^{-7} m^2/s$. Table 1 compares the values obtained by different previous works to the value of diffusivity obtained in our simulation. Berson et al. (2011) have compared the effective diffusivity which is a function of Knudsen number with the bulk diffusivity ($D_eff(Kn)$ $/D_b$) for different Knudsen number flows in a porous medium of porosity 0.3. The bulk diffusivity (D_b) is defined as the diffusivity of the gas where the mean free path of the gas molecules is much smaller than the characteristic length of the pore domain. For gas flows in Knudsen regime with a Knudsen number of

20, the ratio lies between 0.005 to 0.01. The same ratio for the present work is found to be 0.007 which is close to the reported values. The slight variations can be attributed to the difference in porosity values in the present work and the work done by Berson et al. Also, Gunda et al. (2011b) have calculated the ratio D_{eff}/D_o for flows in SOFC electrodes and found the average to be 0.275. In the case of the present work, the ratio is 0.14 which is half the above stated value. Table 4.1 gives an overview of the validation described here.

Based on the size of the pore in which the particle is put and the length of the particle movement, value of the effective diffusivity can change. To account for the spatial variation, the effective diffusivity was calculated by averaging such values for every particle movement in different pore spaces in the domain. The effect of time step on the values of effective diffusivity was studied by changing the length of the particle movement. For every simulation, the length of the movement is fixed in the beginning and the particle is moved for that fixed length. Figure 4.3 below shows the values obtained for the effective diffusivity with different lengths of the particle movement. The effective diffusivity is of the order of 10-9 m2/s for a step length of one and it approaches to the order of $10^{-6}m^2/s$ as we advance the step length to 20. This suggests that the simulations, which cover a fairly good area of the domain, give the correct results for the diffusivity.

4.2.4 Conclusion

Monte Carlo simulations were carried out for a 2D FIB SEM image of SOFC electrode to determine the effective gas diffusivity. The values obtained confirms to the expected values reported in previous works. The results also suggest that the movement of the particles in a discrete fashion along the pixels give a fairly good idea of the diffusivity values. This implies that the 2D images obtained from FIB SEM serve as a good sample for performing simulations rather than numerical construction of artificial random porous geometries which is time consuming and computationally expensive . Further simulations in 3D would be carried out in future to expand the scope of the work.

4.3 Experimental investigations of fluid flow in unstructured microfluidic porous media[2]

Oil reservoir rocks are examples of porous media that contain unstructured porous media. With ever increasing energy demand (Saggaf, 2008) and limited resources for oil and gas, there is a tremendous interest in obtaining the last drop of oil from the established reservoirs. The natural reservoir pressure can produce only around 20 % of original oil in place. Hence additional methods like water flooding and enhanced oil recovery techniques are required to produce significant amount of oil from the reservoirs (Kharrat, 2009; Trivedi and Babadagli, 2009; Yadali Jamaloei et al., 2012). It is beleived that the key driver to displace oil from the reservoir relies on the fact that the oil-water-gas co-exist in the pore-space of the reservoir and one needs to adopt suitable mechanisms to destabilize the oil from the pore space (Blunt, 2001; Blunt et al., 2002; Jamaloei and Kharrat, 2010; Van Dijke et al., 2010). This brings to the focus of this present work, where a new concept in reservoir engineering - Reservoir-on-a-Chip (ROC), developed by Gunda et al. (Gunda et al., 2011a), can be exploited to provide the oil and gas industry with a better tool to understand the pore-scale displacement process relevant to a given geological formation.

Majority of the heavy/light oil is found in carbonate and sandstone formations which consist of solid matrix and pore space. Therefore, the researchers in the past have tried to create micromodels (Karadimitriou and Hassanizadeh, 2012) which consist of regular geometric features with characteristic length-scale comparable with the average pore diameter, quite different than the pore geometry of a natural porous media (Er et al., 2010; Jamaloei and Kharrat, 2010; Wu et al., 2012). However, recent microscopy techniques have made possible to characterize the pore space and pore connectivity of such reservoir rocks (Bera et al., 2011, 2012; Lindquist et al., 2000; Sok et al., 2002; Spanne et al., 1994). In parallel, great advancement of micro/nanofabrication techniques has revolutionized the fabrication of micro-models for energy applications (Berejnov et al., 2008; Fadaei et al., 2011). Building on these two advancements, Gunda et al. (2011a) fabricated the ROC where for the

[2] A version of this section has been submitted for publication in *Lab on a Chip*, September 2012, *In review*

first time the entire pore network of a given reservoir was replicated on a silicon substrate covered with glass. They conducted oil recovery experiments by water flooding technique and were able to comprehensibly understand the displacement process of oil by water within the pore network. This concept of ROC has now been adopted in recent paper by Karadimitriou et al. (2012), where they fabricated a similar pore network on a glass substrate. As ROC is becoming a popular tool to characterize a given reservoir, it is imperative that properties like porosity and permeability need to be calculated for such systems. Hence, in this paper, we have elaborated the technique of calculating relevant reservoir properties, which can be adopted for other types of ROC for different geological formations.

Typically, porosity and permeability are measured in a laboratory scale using core-flooding experimental systems (Hadia et al., 2008; Santosh et al., 2007) and other advanced and sophisticated techniques like X-ray tomography (Dong, 2009; Okabe and Blunt, 2007), Nuclear Magnetic Resonance (Kenyon, 1992; Timur, 1969). Often these techniques are expensive and are difficult to adopt for pore-scale micro-models. Also, there has been an emphasis in extracting pore network information from micro-CT images of sandstone (Al-Kharusi and Blunt, 2007) and carbonate (Okabe and Blunt, 2007) and then using numerical tools (Bakke and Oren, 1997; Hazlett, 1995; Prodanovic et al., 2007) to calculate porosity and permeability of such extracted networks (Arns et al., 2001). However, such technique is limited to the numerical reconstruction method and it is not feasible to visualize the pore-scale displacement process. On the other hand, ROC gives a tremendous flexibility in observing *in situ* pore-scale displacement processes.

In the present work, porosity and permeability are measured for four different pore network structures fabricated on silicon substrates using dry etching. Fabrication procedure for producing such intricate pore network structure has been provided here, which will allow others to replicate the fabrication process relevant to any given extracted pore network. The complete microfluidic chip is fabricated with borofloat glass as covering layer for silicon substrate with proper inlet and outlet for fluidic connections. We characterize the single phase flow properties associated with the ROC consisting of different pore networks. Porosity is determined by processing the optical images of the ROC when it is flooded by the dyed fluid. Permeability is calculated by measuring the pressure drop across the ROC for different flow rates of deionized(DI) water injected

into the ROC. This section starts with a brief description of the technique employed for fabricating the four ROCs. This is followed by a description of the experimental procedures for determination of absolute permeability and porosity. In the next section, results and discussion for the values of porosity and permeability obtained for different ROCs are presented. Further characterization of the ROC in terms of flow resistance for different Darcy numbers is also presented here.

4.3.1 Experimental Investigation

4.3.2 Pore-network Design

Four different pore network ROCs are designed based on the typical sandstone microstructural information. Using Delaunay Triangulation routine (MATLAB, Mathworks Inc., Natick, MA, USA) (Heiba et al., 1982), a pore network of prescribed mean pore size is created for each ROC. Mean pore size of these four networks varies from 40 μm to 70 μm. Network 1 and 2 contain mean pore size of 40 μm, Network 3 contain mean pore size of 70 μm and Network 4 containing mean pore size of 50 μm. The aspect ratio (ratio of pore radius to the linked throat radius) for these networks varies from 1.1 to 6. Coordination number (number of connections of a pore) for these networks varies from 3 to 10, based on total number of pores in the network. The pore and throat sizes are based on beta and log-normal distribution to ensure that the size of the throats in the network are different, which is not the case when only log-normal distribution is used. A combination of beta (Keefer and Bodily, 1983) and log-normal distribution helps in creating varied throat sizes that help in obtaining wider range of entrance pressure in the throats during experiments. Figure 4.4 shows one of the ROCs considered in this work. As observed here, each ROC consists of a pore network, inlet-outlet regions and, entrance and exit regions. The length and width of the pore network part of each ROC is 35 mm and 5 mm, respectively. The entrance and exit regions are rectangular in shape and are of 4.6 mm and 3 mm in length, respectively. The inlet/outlet region is circular in shape and 10 mm in diameter. Table 4.2 provides the number of pores and throats for different ROCs fabricated in the current work and Fig.4.5 shows the nature of the pores and throats, connected with each other through the solid matrices in four separate networks.

4.3.3 Fabrication

This section provides a brief description of the ROC fabrication. Detailed information of ROC fabrication can be found elsewhere (Gunda et al., 2011a). A 4" silicon substrate (Silicon Valley Microelectronics Inc., Santa Clara, CA, USA) is used for etching the pore networks. The silicon substrate is initially cleaned in a piranha solution (H_2SO_4 and H_2O_2 in 3:1 ratio) for 30 minutes and then dried. A 2.5 μm thick layer of positive photo-resist HPR 506 (Fujifilm Electronic Materials Inc., Mesa, Arizona) is spin coated on the substrates followed by the patterning of the pore networks on the positive photo resist with the aid of standard optical lithography process. The silicon substrate is then etched for about $40\mu m$ using inductively coupled plasma reactive ion etching (ICPRIE). The photo-resist is then stripped off using acetone and then properly cleaned using oxygen plasma treatment (Barrel etcher).

A complete ROC is fabricated by closing the open networks in silicon using a glass covering layer. Each ROC has one inlet and outlet port on its covering layer, located centrally with respect to the cicular inlet and outlet regions. The volume of the inlet-outlet regions along with that of the inlet/outlet ports is larger than the volume of the network, and hence, with a suitably chosen volume flow rate, one would achieve laminar flow in the entire pore network. Borofloat glass is selected as the covering material, and holes are drilled using abrasive water-jet machining process. Both the bottom layer with fabricated pore network and the covering top layer are piranha-cleaned again in similar composition as before (H_2SO_4 and H_2O_2 mixture in 3:1). Anodic bonding of the top layer of glass (with inlet and outlet holes) is performed in SUSS Bonder (CB6L, SUSS Microtec, Garching, Germany) with the bottom layer of silicon containing the pore network. Figure 4.6 contains an exploded view of the ROC placed in a microfluidic casing with connecting tubes and O-rings.

Scanning Electron Microscope (ZEISS, Germany) has been used to characterize the open ROC structure before the bonding process. The pore and throat size at various location within the ROC are measured to determine the precision of the network. The fabricated network contains complex connectivity of pores and throats which closely resembles the reservoir characteristics, as observed by Bera et al. (2011, 2012) and others (Lindquist et al., 2000). To further characterize the etched networks, parameters like the mean depth,

width and surface roughness of these networks are measured at several cross-sections of the ROC (entrance and exit regions, inlet-outlet regions and within the network) using surface profilometer (Ambios XP 300, Ambios Technology Inc, Santa Cruz, CA, USA). Table 4.3 compares the average values of these parameters for ROCs. Figure 4.7 shows an example of the surface-profile reading for Network 2. As observed from the figures, the depth of the network remains constant through out the ROC i.e., ~ 42 μm. It is to be noted that the stylus of the profilometer is not able to capture the depth information at the throats whose width is less than 2.5-4 μ m. Hence, the average depth of the etched network measured at other locations were verified from direct measurements of the SEM images.

4.3.4 Experimental setup for porosity and permeability

The experimental setup, as shown in Fig.4.6, consists of a custom made microscope (0.5X-50X magnification, 5M pixel CMOS image sensor) for taking optical images of the ROC when it is flooded with dyed fluid for the purpose of porosity calculation. It is to be noted that the entire network of the ROC needs to be filled with dyed fluid before any kind of measurements are taken and the microscope helps in visualization of the filling of the pore network. The ROC is placed inside a solid casing which contains inlet and outlet ports. The inlet of the ROC is connected to a syringe pump (Harvard Apparatus, MA) which controls the flow of liquid to the ROC. For measuring the inlet pressure, pressure transducer (0-2.5 PSI, 0-5 PSI and 0-15 PSI gauge, Omega Engineering, Inc., Laval,Quebec, Canada) is used at the inlet port of the ROC. The pressure is recorded by using a data acquisition device (DAQ) ($\pm$20 mA/$\pm$10V, 24-Bit Analog Input, National Instruments, Austin, TX, USA).

The ROC is firmly placed inside the solid casing and care is taken that no leakage occurs during the liquid flow by placing O-rings at the interface between inlet and outlet ports of the casing and the ROC. Teflon tubing is selected to connect the syringe pump, the pressure transducer and the ROC. The electric terminals of the pressure transducer are connected to the DAQ device which is then connected to a computer. Water is injected by the syringe pump at different appropriate flow rates.

The porosity of the ROCs was determined using the image analysis tech-

nique. Authors in the past have mentioned about the difficulty in measuring porosity by using experimental material balance procedures in micro-models (Buchgraber et al., 2012). Image analysis is a simple and less time consuming method for calculating porosity compared to the material balance calculations. The images of each ROC were obtained along the length of its network using the microscope after flooding it with a white colored dye. For clarity and demonstration purpose, a part of the whole image of Network 3 is shown in Fig.4.8. The image analysis technique mainly consists of three steps, namely normalization, segmentation or thresholding and filtering. The obtained images of the ROC are first converted to 8 bit images from 16 bit, which render them as grey scale images, by importing them into the image processing software FIJI (Open Source image processing package based on ImageJ). This is followed by the normalization process for improving the resolution and contrast of the 8 bit images which includes changing the range of pixel intensity values. A normalized image is shown in Fig.4.8(b). These normalized images are then segmented for clear distinction between different phases. The different phases are distinguished and identified based on the intensity of its pixels by adjusting the threshold of the intensity of the pixels. For the images obtained in this experiment, the threshold value changes based on the individual image. An example of an image after thresholding of its pixel intensity can be seen in Fig.4.8(c), where the threshold value is 49. The pixels that have a value below 49 are kept as black and ones that were above 49 are kept as white. The black color in the Fig.4.8(c) represents the solid matrix and the white color refers to the pore space. The images are then smoothened by applying median filter to reduce any noise and is shown in Fig.4.8(d). A detailed description of the image processing method can be found elsewhere (Gunda et al., 2011b). Once the noise in the image is reduced, it is then imported to MATLAB and is converted to a binary image, which contains the information of black and white pixels as 0s and 1s, respectively. Porosity is calculated by counting the number of pixels that represent the pore space and dividing it by the total number of pixels.

The absolute permeability is determined by injecting deionized water through the ROC at different flow rates and measuring the corresponding pressure drop across the pore network length. Once the pressure drop is recorded, the permeability is calculated by using Darcy's law which is given by (Dullien, 1992):

$$K = \frac{Q \times \mu \times L}{A \times \Delta P} \tag{4.6}$$

where K is the permeability, Q is the flow rate of water, μ is the viscosity of water, L is the length of the porous network, A is the flow cross sectional area which is the product of the width (W) and height (h) of the ROC and ΔP is the pressure difference across the pore network. It is important to consider different pressure drops that occur during the flow in the experimental setup described here. The total pressure drop is given by(Akbari et al., 2009):

$$\Delta P_{total} = \Delta P_{C,I} + \Delta P_{C,O} + \Delta P_D + \Delta P_{FD} + \Delta P_{minor} + \Delta P_{ev} \tag{4.7}$$

where $\Delta P_{C,I}$ is the pressure loss in the inlet tube between the pressure transducer and the inlet port of the ROC, $\Delta P_{C,O}$ is the pressure drop in the outlet tube connected to the outlet port of the ROC, ΔP_D comprises of the pressure drop in the entrance region where the flow is still not fully developed and in the exit region right after the pore network, ΔP_{FD} is the pressure drop in the fully developed region of the pore network, ΔP_{minor} is the pressure drop due to the 90° bends at the inlet and the outlet ports and due to the sudden expansion and contraction at the inlet and outlet ports respectively, and ΔP_{ev} is the pressure drop due to electroviscous effect. The pressure loss in the inlet and outlet tubes, $\Delta P_{C,I}$ and $\Delta P_{C,O}$ respectively, have been calculated using the Hagen-Poiseuille equation for pressure drops in a tube and have been included in the net pressure drop while calculating the permeability values. ΔP_D has been calculated for the entrance and exit regions which are rectangular in shape with the same width and height but different length as that of the ROC. ΔP_{minor} can be ignored as they are calculated to be very less (of the order of 10^{-3} Pa) and ΔP_{ev} can be ignored for rectangular ROC used in the present work. Details for calculating such pressure drops can be found elsewhere (Akbari et al., 2009).

Due to the variation in flow rates and the time taken to attain steady state flow in each case, errors and uncertainties can occur during the pressure drop measurement and hence in the permeability calculation. Pressure drop measurements for each ROC are repeated three times and the flow rates are varied between 50μL to 500μL. The readings were taken once the temporal fluctuations in the pressure transducer voltage readings were stabilized. The final value of the pressure drops for each ROC was the mean of these three measurements.

4.4 Results and discussion

The porosity measurement data for the different ROCs are given in Table 4.4. The four different ROC networks that we created represent porous media over a wide range of porosity. Apart from calculating porosity from image analysis presented in the earlier section, the porosity of the networks were also calculated using the design images(AUTOCAD drawing file), one of which is shown in Fig.4.4. This was done to distinguish between the true porosity of the network and the effective porosity after etching. The fabricated networks may contain isolated or dead end pores (due to some inaccuracies of the fabrication process) and may result into a reduced value of porosity as compared to the true porosity. The design images were imported to MATLAB and the porosity was calculated by counting the number of pixels that belonged to the pore space and dividing it by the total number of pixels. A comparison of the porosity obtained from image analysis with the porosity of the design images is provided in the Table 4.4. There is a slight variation between the two porosity values. In general, porosity varies between the least dense network (Network 1: design porosity - 0.42, ROC porosity - 0.39, error - 7%) to the most dense network (Network 4: design porosity - 0.69, ROC porosity - 0.67, error - 2%). The deviations could occur due to the difference in thresholding limits that have been applied to the optical images of the networks. To determine the effect of thresholding on the values of porosity, the images were processed for porosity calculation within $\pm$ 5 % of the base thresholding limit. Table 4.4 provides the variation in the effective porosity values, obtained by image analysis, due to the change in thresholding limits applied.

Figure 4.9 presents the variation of the pressure drop with flow rate for four different ROCs. It is observed that the pressure drop increases with the flow rate. It is also found that the, Network 1 has higher pressure drop values for different flow rates. As the porosity increases, the slope of the pressure gradient line decreases thus signifying less resistance to the flow. Network 4, which has the maximum porosity, develops the least pressure drop values.

Permeability values for the four different ROCs are shown in the Table 4.4. The permeability varies between 2.66-16 Darcys and the error estimates have been provided in the Table 4.4. As expected, the Network 1 has the least

permeability due to lowest porosity. Network 4 has the highest permeability as it contains the maximum number of pores and throats. Though Network 1 and Network 2 contain the same average pore size, permeability in Network 2 is two times that of Network 1 due to the increase in number of pores and throats. The same trend is seen in permeability change from Network 2 to Network 3 where the number of pores and throats remain the same but the average pore size increases from 40 μm to 70 μm. The increase in permeability from Network 3 to Network 4 is not as much as seen in the previous trends even though the number of throats and pores have increased with a reduction in the average pore size. Overall, with increase in porosity values for the ROCs from 0.39 to 0.67, the permeability increase is approximately of one order of magnitude.

Figure 4.10 represents the variation of flow resistance, $\Delta P/L\mu U$, offered by different ROC networks as the flow rate increases. Here μ is the viscosity of DI water, which is 1 $\times 10^{-3}$ Pa s, U is the velocity which is obtained by dividing the flow rate Q with the cross sectional area A of the ROC and L is the length of the network, which is 35mm. It is evident from the figure that Network 1 offers the maximum resistance to flow due to the least porosity and Network 4 offers the least resistance. Figure 4.11 shows another indication of the resistance to flow, given by the ratio of pressure drop to the flow rate value ($\Delta P/Q$), with varying Darcy number ($\sqrt{K/h^2}$). Here K is the permeability of the ROC, which has been obtained experimentally and h is the height of the etched network, which is 42 μm for all the networks. As seen in Fig.4.10, the flow resistance is maximum for the network with the least porosity (Network 1) and is minimum for the network with the maximum porosity (Network 4). The flow resistance gradually decreases as the porosity increases in the network.

4.5 Conclusion

In this work, a novel microfluidic chip i.e., Reservoir-On-a-Chip (ROC) was fabricated and characterized using SEM and surface profilometer. Four different types of ROCs varying in number of pore bodies and pore throats were considered in this work. Properties like porosity and permeability were calculated to understand the porous behavior of different ROCs. Image analysis

technique was used to determine the porosity of the ROCs and the porosity values ranged between 0.39 to 0.67. Pressure drops across the pore networks were measured and were used for calculating permeability values. It was observed that as the flow rate increased, the pressure drop increased linearly in the networks. The flow resistance was maximum for Network 1 and was minimum for Network 4. It was also seen that the resistance to flow offered by the networks decreases with increase in Darcy number. Permeability for each of the ROCs was calculated and was found to be ranging between 2.66 and 15.93 Darcys. It is concluded that the quantification of these properties would help in future studies of enhanced oil recovery conducted in ROC pore networks.

Table 4.1 – Validation of numerical results with theoretical works

Validation A	D_{eff}/D_b
Berson et al. (2011)	0.005-0.01
Current work	0.007
Validation B	D_{eff}/D_o
Bruggeman Equation	0.42
Gunda et al. (2011b)	0.275
Current work	0.14

Table 4.2 – Pore and throat number of various ROC networks

Network type	**Number of Pores**	**Number of throats**
Network 1	2000	6000
Network 2	3000	9000
Network 3	3000	9000
Network 4	6000	20000

Table 4.3 – Surface profile properties (width, average roughness and average depth) of fabricated ROCs

Network	**Width of the ROC**(mm)	**Average roughness** (μm)	**Average depth** (μm)
1	4.89	4.54	40.44
2	4.95	6.17	40.76
3	4.96	5.24	41.44
4	4.96	6.67	41.10

Table 4.4 – Porosity and permeability values of different ROCs

Network type	**Design porosity**	**Porosity from optical images**	**Permeability (Darcy)**
Network 1	0.42	0.39 ± 0.04	2.66 ± 0.06
Network 2	0.44	0.42 ± 0.04	5.50 ± 0.40
Network 3	0.66	0.65 ± 0.05	10.88 ± 1.03
Network 4	0.69	0.67 ± 0.03	15.93± 0.55

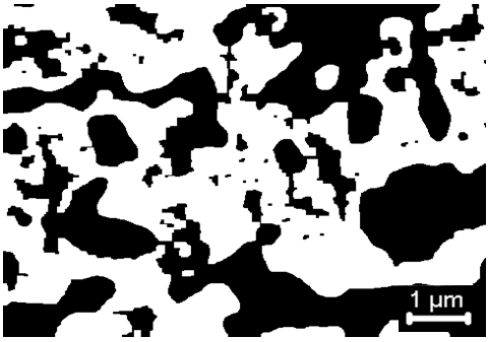

Figure 4.1 – 2D image of an SOFC electrode cross section obtained using FIB-SEM

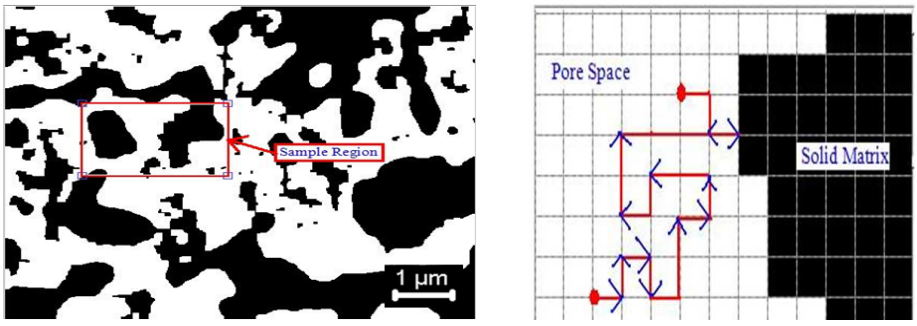

(a) (b)

Figure 4.2 – (a) Sample region comprising of solid matrix and pore space (b) Particle movement in the porous medium domain

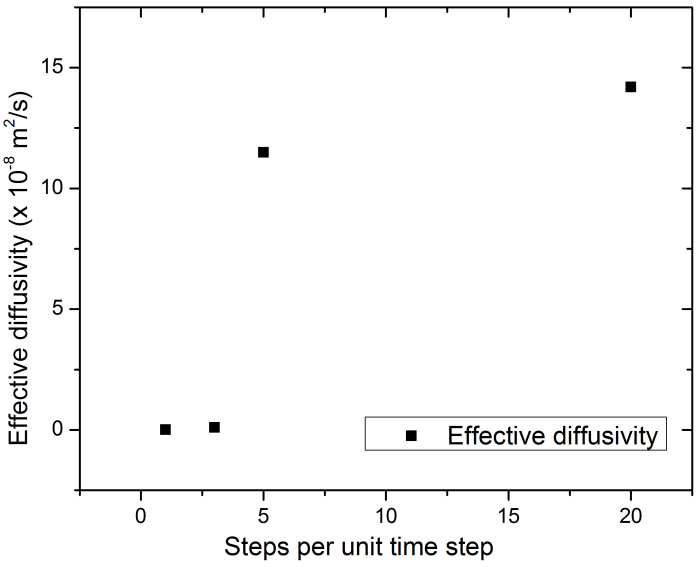

Figure 4.3 – Variation of effective diffusivity values with varying particle movement lengths

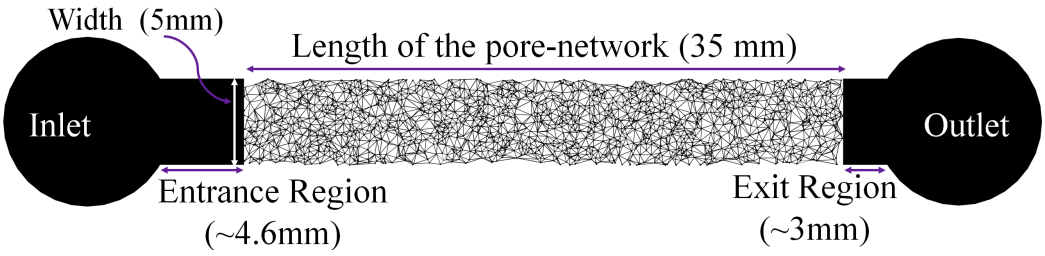

Figure 4.4 – ROC with pore network, entrance and exit regions and circular inlet/outlet regions.

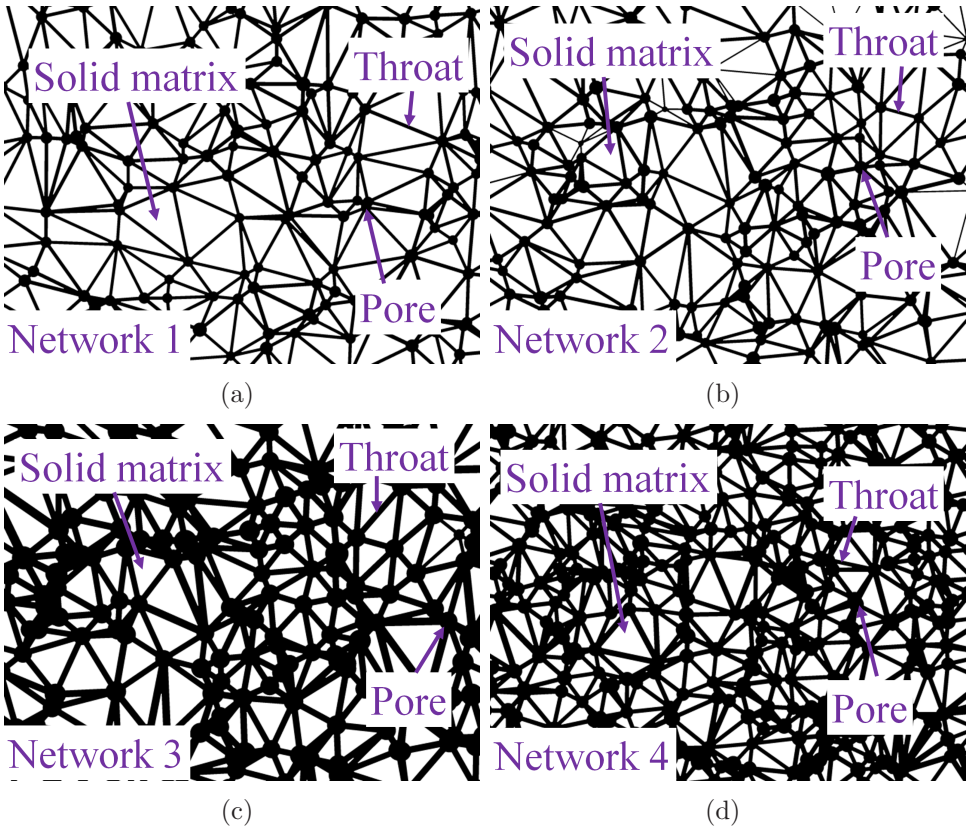

Figure 4.5 – Different types of pores and throats for four different ROCs; (a) Network 1, (b) Network 2, (c) Network 3 and (d) Network 4

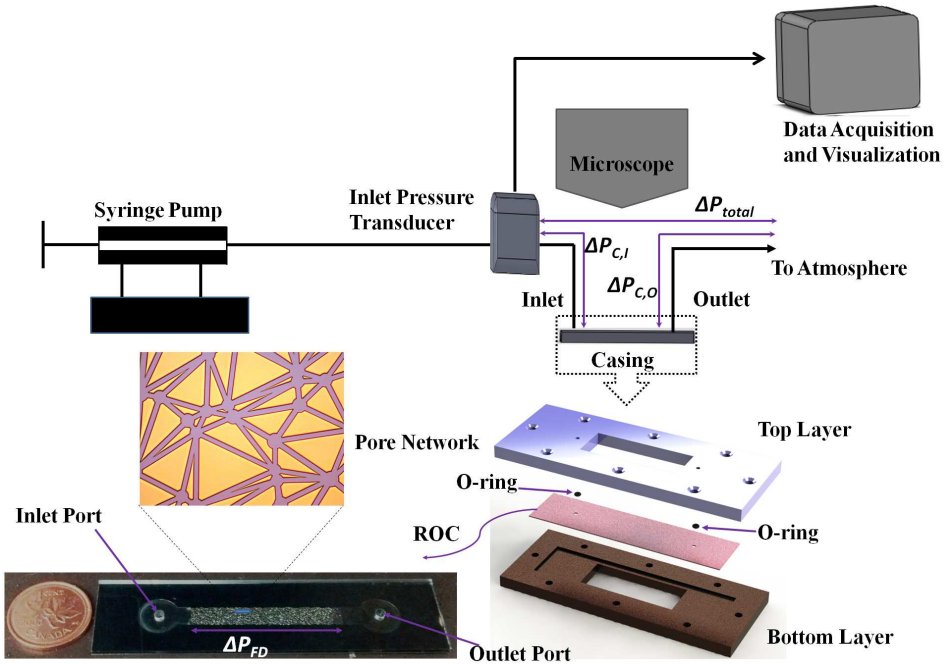

Figure 4.6 – Schematic of the experimental set-up considered for porosity and permeability measurements in ROC.

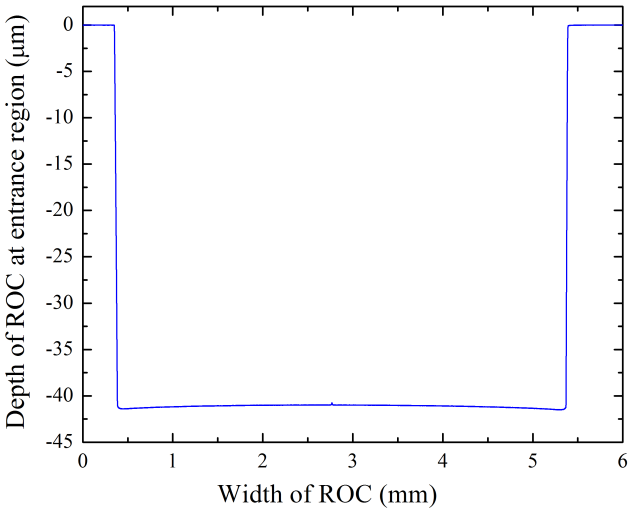

(a)

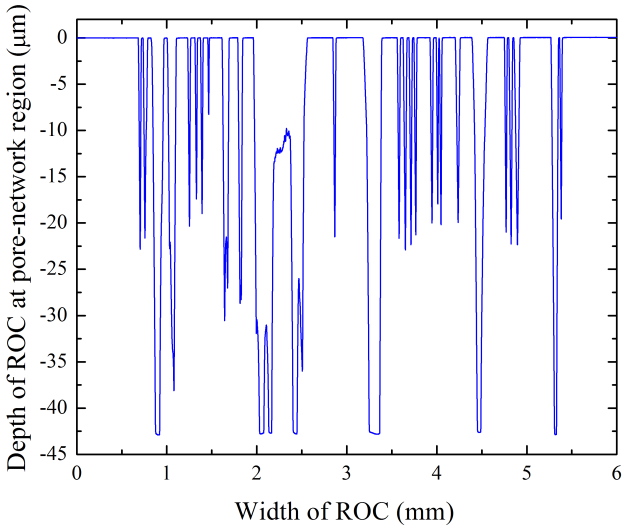

(b)

Figure 4.7 – Surface profile for Network 2; (a) At entrance; (b) Inside the network

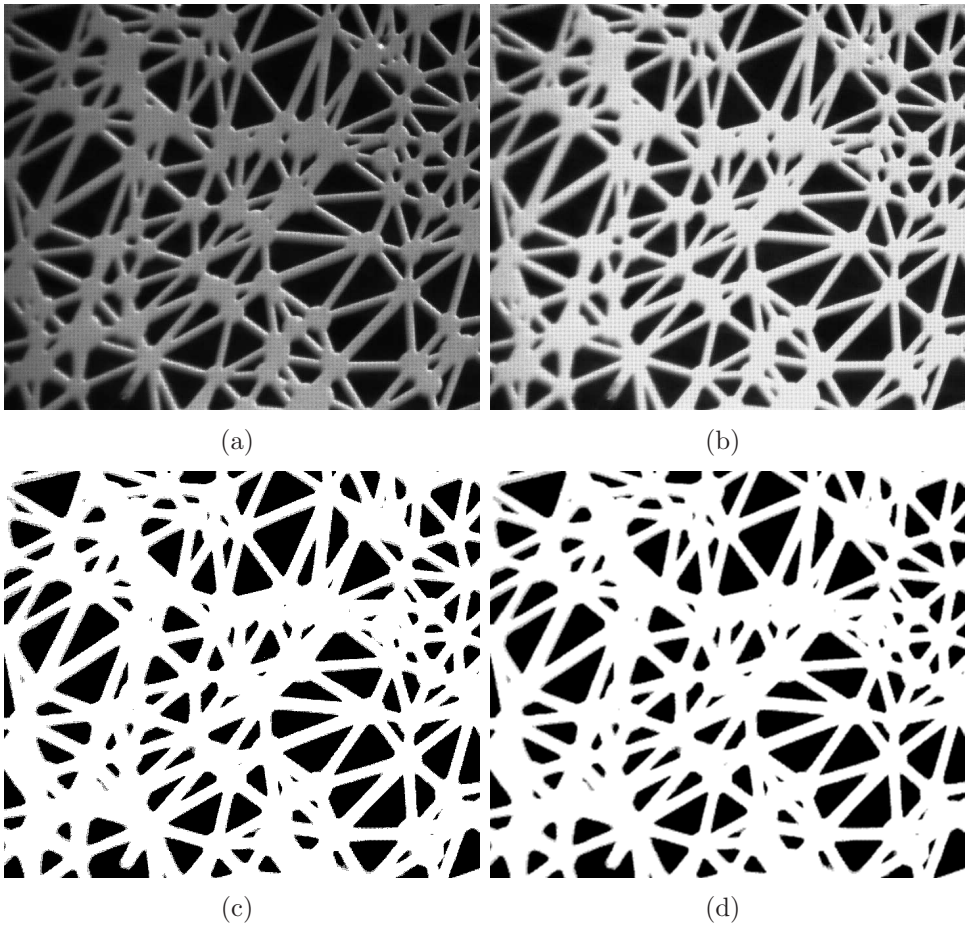

Figure 4.8 – A part of the image of Network 3 is shown here for the purpose of explaining the porosity calculation procedure; (a) 8 bit optical image; (b) Normalized image with better resolution and contrast; (c) Image after thresholding; and (d) Thresholded image after filtering.

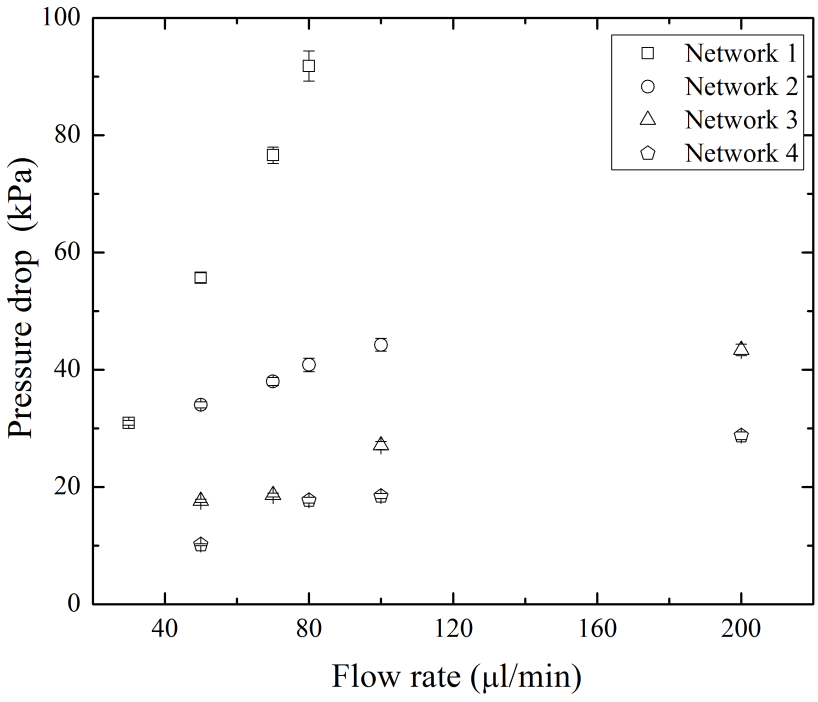

Figure 4.9 – Variation of pressure drop with flow rates for different ROC networks.

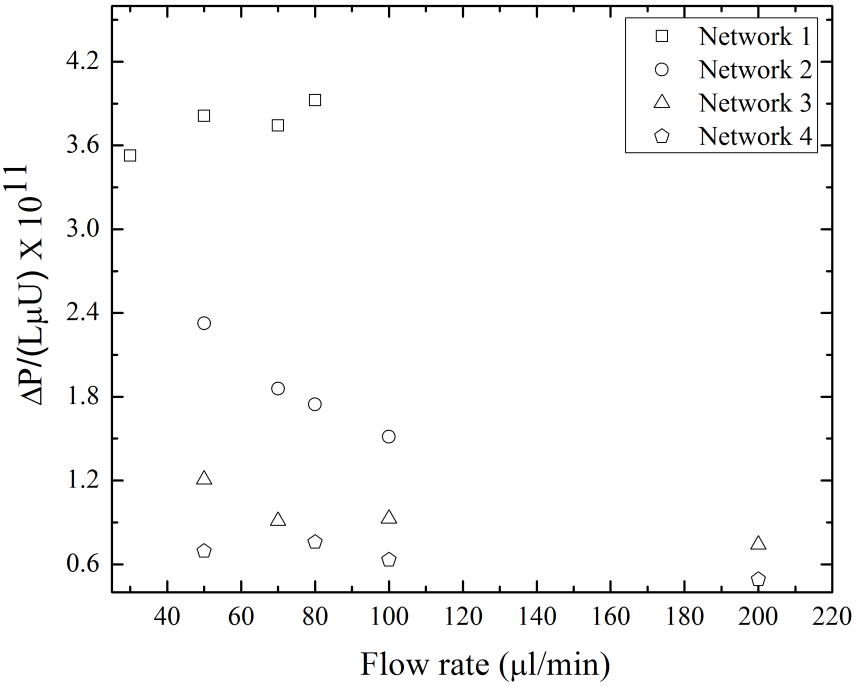

Figure 4.10 – Flow resistance developed in different ROC networks for different flow rates.

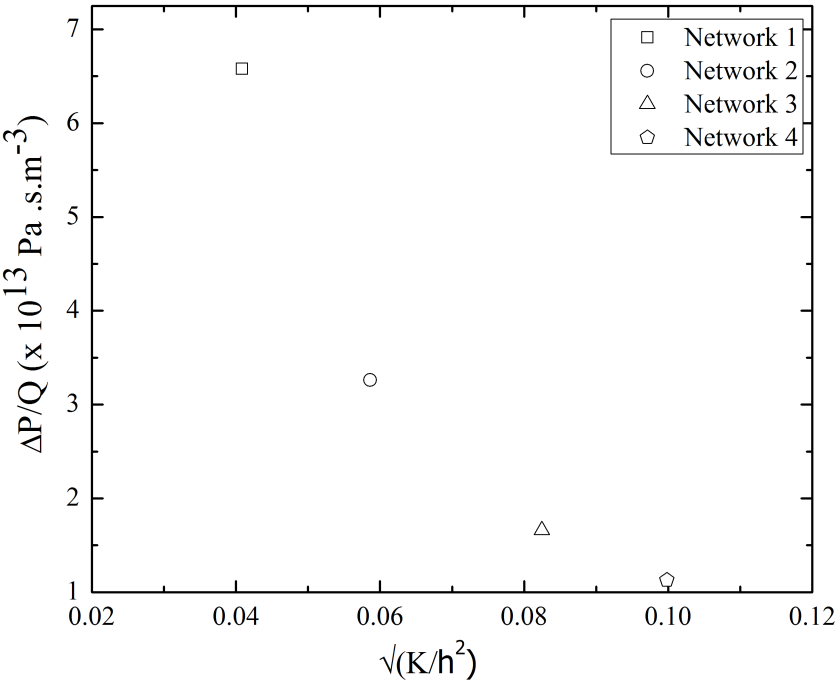

Figure 4.11 – Variation of pressure drop per unit flow with change in Darcy number for different ROC networks.

References

M. Akbari, D. Sinton, and M. Bahrami. Pressure drop in rectangular microchannels as compared with theory based on arbitrary cross section. *Journal of Fluids Engineering, Transactions of the ASME*, 131(4):0412021–0412028, 2009.

A S Al-Kharusi and M J Blunt. Network extraction from sandstone and carbonate pore space images. *Journal of Petroleum Science and Engineering*, 56(4):219–231, 2007.

C.H. Arns, M.A. Knackstedt, W. Val Pinczewski, and W.B. Lindquist. Accurate estimation of transport properties from microtomographic images. *Geophysical Research Letters*, 28(17):3361–3364, 2001.

S Bakke and P E Oren. 3-d pore-scale modelling of sandstones and flow simulations in the pore networks. *SPE Journal*, 2(2):136–149, 1997.

B Bera, S K Mitra, and D Vick. Understanding the micro structure of berea sandstone by the simultaneous use of micro-computed tomography (micro-CT) and focused ion beam-scanning electron microscopy (FIB-SEM). *Micron*, 42(5):412–418, 2011.

B. Bera, N. S. K. Gunda, S. K. Mitra, and D. Vick. Characterization of nanometer-scale porosity in reservoir carbonate rock by focused ion beam scanning electron microscopy. *Microscopy and Microanalysis*, 18(01):171–178, 2012.

V Berejnov, N Djilali, and D Sinton. Lab-on-chip methodologies for the study of transport in porous media: Energy applications. *Lab on a Chip*, 8(5): 689–693, 2008.

A. Berson, H.-W. Choi, and J.G. Pharoah. Determination of the effective gas diffusivity of a porous composite medium from the three-dimensional reconstruction of its microstructure. *Physical Review E - Statistical, Nonlinear, and Soft Matter Physics*, 83(2), 2011.

M.J. Blunt. Flow in porous media-pore network models and multiphase flow. *Current Opinion in Colloid and Interface Science*, 6:197–207, 2001.

M.J. Blunt, M.D. Jackson, M. Piri, and P.H. Valvatne. Detailed physics, predictive capabilities and macroscopic consequences for pore-network models of multiphase flow. *Advances in Water Resources*, 25:1069–1089, 2002.

V.D.A.G. Bruggeman. Berechnung verschiedener physikalischer konstanten von heterogenen substanzen. *Annalen der Physik*, 416(7):636–664, 1935.

M. Buchgraber, M. Al-Dossary, C.M. Ross, and A.R. Kovscek. Creation of a dual-porosity micromodel for pore-level visualization of multiphase flow. *Journal of Petroleum Science and Engineering*, 86-87:27–38, 2012.

A. Cancelliere, C. Chang, E. Foti, D.H. Rothman, and S. Succi. The permeability of a random medium: Comparison of simulation with theory. *Physics of Fluids A*, 2(12):2085–2088, 1990.

S. Chandrasekhar. Stochastic problems in physics and astronomy. *Reviews of Modern Physics*, 15(1):1–89, 1943.

Blunt M.J. Dong, H. Pore-network extraction from micro-computerized-tomography images. *Physical Review E*, 80(3), 2009.

F.A.L. Dullien. *Porous media: fluid transport and pore structure*, volume 26. Academic press, 1992.

A. Einstein. *Investigation on the theory of the Brownian Movement*. Dover Publications, 1956.

V. Er, T. Babadagli, and Z. Xu. Pore-scale investigation of the matrix-fracture interaction during co 2 injection in naturally fractured oil reservoirs. *Energy and Fuels*, 24(2):1421–1430, 2010.

H. Fadaei, B. Scarff, and D. Sinton. Rapid microfluidics-based measurement of co 2 diffusivity in bitumen. *Energy and Fuels*, 25(10):4829–4835, 2011.

D. Frenkel and B. Smit. *Understanding Molecular Simulation: From Algorithms to Applications*. Academic Press, Inc., 1996.

N.S.K. Gunda, B. Bera, N.K. Karadimitriou, S.K. Mitra, and S.M. Hassanizadeh. Reservoir-on-a-chip (roc): A new paradigm in reservoir engineering. *Lab on a Chip*, 11(22):3785–3792, 2011a.

N.S.K. Gunda, H.-W. Choi, A. Berson, B. Kenney, K. Karan, J.G. Pharoah, and S.K. Mitra. Focused ion beam-scanning electron microscopy on solid-oxide fuel-cell electrode: Image analysis and computing effective transport properties. *Journal of Power Sources*, 196(7):3592–3603, 2011b.

N.J. Hadia, L.S. Chaudhari, S.K. Mitra, M. Vinjamur, and R. Singh. Effect of scaling parameters on waterflood performance with horizontal and vertical wells. *Energy and Fuels*, 22(1):402–409, 2008.

C.U. Hatiboglu and T. Babadagli. Lattice-boltzmann simulation of solvent diffusion into oil-saturated porous media. *Physical Review E - Statistical, Nonlinear, and Soft Matter Physics*, 76(6), 2007.

R.D. Hazlett. Simulation of capillary-dominant displacements in microtomographic images of reservoir rocks. *Transport in Porous Media*, 20:21–35, 1995.

A A Heiba, M Sahimi, L E Scriven, and H Ted Davis. Percolation theory of two-phase relative permeability. 1982.

S. Jain, M. Acharya, S. Gupta, and A.N. Bhaskarwar. Monte carlo simulation of flow of fluids through porous media. *Computers and Chemical Engineering*, 27(3):385–400, 2003.

B.Y. Jamaloei and R. Kharrat. Analysis of pore-level phenomena of dilute surfactant flooding in the presence and absence of connate water saturation. *Journal of Porous Media*, 13(8):671–690, 2010.

N. K Karadimitriou and S. Hassanizadeh. *Vadose Zone Journal*, 2012.

N. K. Karadimitriou, V.J. Niasar, S. M. Hassanizadeh, Kleingeld P. J., and L. J. Pyrak-Nolte. A novel deep reactive ion etched (drie) glass micro-model for two-phase flow experiments. *Lab Chip*, 12:3413–3418, 2012.

D L Keefer and S E Bodily. Three-point approximations for continuous random variables. *Management Science*, 29(5):595–609, 1983.

E.H. Kennard. *Kinetic theory of gases: with an introduction to statistical mechanics*. McGraw-Hill New York, 1938.

W E Kenyon. Nuclear magnetic resonance as a petrophysical measurement. *Nuclear Geophysics*, 6(2):153–171, 1992.

A.M. Kharrat. Characterization of canadian heavy oils using sequential extraction approach. *Energy and Fuels*, 23(2):828–834, 2009.

D.P. Landau and K. Binder. *A guide to Monte Carlo simulations in statistical physics*. Cambridge University Press, 2005.

W.B. Lindquist, A. Venkatarangan, J. Dunsmuir, and T.-F. Wong. Pore and throat size distributions measured from synchrotron x-ray tomographic images of fontainebleau sandstones. *Journal of Geophysical Research B: Solid Earth*, 105(B9):21509–21527, 2000.

H. Okabe and M.J. Blunt. Pore space reconstruction of vuggy carbonates using microtomography and multiple-point statistics. *Water Resources Research*, 43(12), 2007.

M. Prodanovic, W.B. Lindquist, and R.S. Seright. 3d image-based characterization of fluid displacement in a berea core. *Advances in Water Resources*, 30(2):214–226, 2007.

M.M. Saggaf. A vision for future upstream technologies. *Journal of Petroleum Technology*, 60(3):54–55+94–98, 2008.

M. Sahimi and D. Stauffer. Efficient simulation of flow and transport in porous media. *Chemical Engineering Science*, 46(9):2225–2233, 1991.

V. Santosh, S.K. Mitra, M. Vinjamur, and R. Singh. Experimental and numerical investigations of waterflood profiles with different well configurations. *Energy and Fuels*, 21(6):3353–3359, 2007.

R.M. Sok, M.A. Knackstedt, A.P. Sheppard, W.V. Pinczewski, W.B. Lindquist, A. Venkatarangan, and L. Paterson. Direct and stochastic generation of network models from tomographic images; effect of topology on residual saturations. *Transport in Porous Media*, 46(2-3):345–372, 2002.

P. Spanne, J.F. Thovert, C.J. Jacquin, W.B. Lindquist, K.W. Jones, and P.M. Adler. Synchrotron computed microtomography of porous media: Topology and transports. *Physical Review Letters*, 73(14):2001–2004, 1994.

A. Timur. Pulsed nuclear magnetic resonance studies of porosity, movable fluid, and permeability of sandstones. *J Petroleum Technology*, 21(6):775–786, 1969.

Manolis M. Tomadakis and Stratis V. Sotirchos. Ordinary and transition regime diffusion in random fiber structures. *AIChE Journal*, 39(3):397–412, 1993.

J.J. Trivedi and T. Babadagli. Oil recovery and sequestration potential of naturally fractured reservoirs during co2 injection. *Energy and Fuels*, 23(8): 4025–4036, 2009.

M.I.J. Van Dijke, M. Lorentzen, M. Sohrabi, and K.S. Sorbie. Pore-scale simulation of wag floods in mixed-wet micromodels. *SPE Journal*, 15(1): 238–247, 2010.

M.A. van Doormaal and J.G. Pharoah. Determination of permeability in fibrous porous media using the lattice boltzmann method with application to pem fuel cells. *International Journal for Numerical Methods in Fluids*, 59(1):75–89, 2009.

M. Wu, F. Xiao, R.M. Johnson-Paben, S.T. Retterer, X. Yin, and K.B. Neeves. Single- and two-phase flow in microfluidic porous media analogs based on voronoi tessellation. *Lab on a Chip - Miniaturisation for Chemistry and Biology*, 12(2):253–261, 2012.

B. Yadali Jamaloei, M. Dong, N. Mahinpey, and B.B. Maini. Enhanced cyclic solvent process (ecsp) for heavy oil and bitumen recovery in thin reservoirs. *Energy and Fuels*, 26(5):2865–2874, 2012.

Chapter 5

Conclusion and Future Work

5.1 Concluding Remarks

The aim of this research was to conduct experimental investigations for determining various transport properties in microfluidic porous media. In order to achieve this objective, fluid flow through microfluidic devices that contained porous media was studied. Measurements of pressure drop resulting from the fluid flow in such devices were done and transport properties like permeability were calculated. For the present study, microfluidic porous media representing a wide range of practical applications were selected. De-ionized water was injected into the microfluidic devices at small flow rates so that laminar flow was obtained.

At first, pressure drop and the resulting flow resistance were measured experimentally for single phase liquid flow in microchannels with integrated micropillars (MCIPs). These microfluidic devices have immense importance in many practical engineering applications such as micro cooling, micro filtration, compact heat exchangers and fuel cells. The microfluidic devices, containing integrated cylindrical micro pillars, were fabricated using deep reactive ion etching (DRIE) and the micro pillars were arranged in square and staggered arrangements. Pressure drop measurements were done in these microfluidic devices that represented micro pillar arrangements over a wide range of porosity. The pressure drop increased linearly with increasing flow rates in all the MCIPs. The Darcy number in the fabricated devices ranged between 0.05 and 0.31. Flow resistance was obtained from the pressure drop values and was found that the square arrangement of pillars offered higher resistance to flow compared to their staggered counterparts. The flow resistance decreased

with increasing Darcy number in both the pillar arrangements. In general, with increasing diameter and hence decreasing porosity, the resistance to flow increased. Permeabilities of the different microfluidic devices with integrated micropillars with square and staggered arrangement were obtained from the pressure drop values using Darcys law. It is found that the available theoretical models, that predict pressure drop and permeabilities in such microchannels filled with cylindrical pillars, are not sufficient to predict the experimental values obtained as the two are in considerable deviations.

Further to the experiments in structured microfluidic porous media, we extended the studies to unstructured porous media that was built on microfluidic devices using DRIE techniques. Prior to attempting experimental investigations, we demonstrate Monte Carlo simulation technique that can be used for solving porous media flow problems in cases where the geometry is too complex or when there are little analytical results available such as in the case of unstructured microfluidic porous media considered here. This type of microfluidic porous media, known as Reservoir-On-a-Chip, mimics the pore structure of a naturally occurring reservoir rock and hence is highly usefulto study pore scale transport phenomena in such reservoirs at lab scale. The pore networks obtained by anisotropic etching of silicon wafers were $40m$ deep and had smooth and vertical wall profiles. This microfluidic device contained pore networks which mimicked the actual porous media as compared to the idealistic representations such as random sphere of spheres which were used in the past. Also, the glass etching process is replaced by etching on silicon which results in better pore throat and pore body representations. Four different networks varying in the number of pore bodies and pore throats were fabricated and important petrophysical properties like porosity and permeability were calculated. Image analysis technique was employed to obtain porosity and was found to be varying from 0.39 to 0.67. Permeabilities for these four different ROCs were determined by measuring pressure drop across the inlet and outlet of the porous media and applying Darcys law. The permeability values ranged between 2.66 and 15.93 Darcy. As expected, the microfluidic device which large number of throats and pores is the most permeable model showing good interconnection between pores. In summary, this thesis presents:

- Single phase fluid flow experiments in both structured and unstructured porous media contained in microfluidic devices.

- Pressure drop and flow resistance quantified for structured microfluidic porous media represented by microchannels with integrated micropillars (MCIPs).
- Monte Carlo simulations to calculate effective transport properties at small length scales in realistic porous media images.
- Estimation of porosity and permeability in unstructured porous media enclosed in a microfluidic device that has got wide applications in oil recovery and en- enhanced extraction.
- Preliminary evidence of deviations from the available theoretical models for structured microfluidic porous media flows.

5.2 Future Work

The present work quantified transport properties, such as pressure drop and permeability, in microfluidic porous media. Though this study is helpful in understanding pore scale phenomena, it is also important to know how microscale properties could be used to determine properties at field scale with application to oil recovery, underground water transport etc., something which is not attempted in this study. This could be an exciting work which would help in moving from pore scale to lab scale and ultimately to field scale.

Another continuation of this work could be the experimental investigation of two and three phase flows in such microfluidic devices. Study of multiphase flows are found in practical applications like oil recovery, enhanced oil recovery techniques, NAPL transport in porous media and it is important to understand such multiphase flows in pore scale using the advanced microfluidic porous media devices. For example, knowledge of relative permeability curves in such microfluidic porous media would help to understand the relative permeability in micro scale flows. Also, numerical recipies could be developed for multiphase flows in realisitic 3D porous media images as opposed to the 2D image used in the present work. Such studies would help to provide data for further simulation and understanding of micro scale studies attended in porous media for numerous engineering applications.

Appendix A

Pressure Drop Measurements[1]

This appendix explains the various pressure drop measurements associated with microfluidic experiments done in chapter 3 and 4. Below is an example for the pressure drop calculations performed for chapter 3. Similar pressure drop calculations have been performed for chapter 4.

A.1 Pressure drop calculation for MCIP

The total pressure drop measured in the experiment is given by:

$$\Delta P_{total} = \Delta P_{C,I} + \Delta P_{C,O} + \Delta P_D + \Delta P_{FD} + \Delta P_{minor} + \Delta P_{ev} \tag{A.1}$$

where $\Delta P_{C,I}$ is the pressure loss in the inlet tube between the pressure transducer and the inlet port of the microchannel and $\Delta P_{C,O}$ is the pressure drop in the outlet tube connected to the outlet port of the microchannel. The pressure drop in the tubing is calculated by using Hagen-Poiseuille equation, which is given as:

$$\Delta P_{C,I/O} = \frac{8\mu LQ}{\pi R^4} \tag{A.2}$$

where μ is the visocity of the fluid, L is the length of the tube, Q is the flow rate and R is the radius of the tube. In the present work, 1/16 inch tubes with the length of 5 cm each were used. The pressure drop for both the tubes has been calculated and is provided in Table A.1 of the supplementary document.

In Eq.(A.1), ΔP_D refers to the combined pressure drop in the entrance and exit regions of the MCIPs. Both these regions are rectangular in shape with

[1]This appendix has been included as supplementary material for chapter 3 which is submitted for publication in *Microfluidics and Nanofluidics*, August 2012, *In review*

the same width and height but different length as that of the microchannel. The pressure drop associated in these regions is provided in Table A.2 of this supplementary document. Details for calculating such pressure drops can be found elsewhere (Akbari et al., 2009).

In Eq.(A.1), ΔP_{minor} is the pressure drop in the inlet and the outlet ports of the microfluidic channel. The inlet and outlet ports of the channel are circular in cross section with a diameter of 2.1 mm and a length of 1.098 mm. The pressure drop in these ports can be calculated similar to Eq. A.2 and are found to be of the order of $\sim$ 0.0068 Pa for the highest flow rate and hence can be neglected.

In Eq.(A.1), ΔP_{ev} is the pressure drop due to electroviscous effect which occurs in pressure driven flows in very narrow channels. Due to the electroviscous effects, there is an apparent increase in the fluid viscosity. Akbari et al. (2009) have reported that the ratio of apparent viscosity and the actual viscosity is almost unity for the type of rectangular microchannels used in this study. Hence ΔP_{ev} can be ignored.

The quantity which is measured in the experiment is the ΔP_{total}, the left hand side of Eq.(A.1). As discussed here, all terms in right hand side of Eq.(A.1) is known, except ΔP_{FD}. Based on Eq.(A.1), then actual pressure drop across the MCIP, ΔP_{FD}, is calculated.

Table A.1 – Combined pressure drop ($\Delta P_{C,I} + \Delta P_{C,O}$) in the inlet and the outlet tubings.

Flow rate ($\mu l/min$)	$\Delta P_{C,I} + \Delta P_{C,O}$(Pa)
50	0.5343
80	0.8549
100	1.0691
200	2.1381
300	3.2072
400	4.2762
600	6.4143

Table A.2 – Combined pressure drop (ΔP_D) at entrance and exit regions of different arrangements of MCIP.

Arrangement	ΔP_D(Pa)						
	$50(\mu l/min)$	$80(\mu l/min)$	$100(\mu l/min)$	$200(\mu l/min)$	$300(\mu l/min)$	$400(\mu l/min)$	$600(\mu l/min)$
NSq 95-30	-	-	-	32.2563	48.3845	64.5126	96.7679
NSq 90-30	20.2422	32.3874	40.4842	80.9684	121.4525	161.9372	-
NSq 80-50	12.7764	20.4422	25.5528	51.1057	76.6585	-	-
NSq 70-50	14.0905	22.5449	28.1811	56.3622	-	-	-
NSq 50-100	9.6530	15.4448	19.3060	38.6120	-	-	-
NSt 90-30	-	28.9843	36.2304	72.4609	108.6903	144.9223	-
NSt 80-50	17.6161	28.1878	35.2348	70.4696	105.7045	-	-
NSt 70-50	22.5050	36.0080	45.0089	90.0193	135.0299	-	-
NSt 50-100	18.4211	29.4738	36.8423	73.6847	110.5269	-	-

Appendix B

Error Estimates[1]

We report here the error estimates associated with the the experimental calculations performed in chapter 3. Similar estimates were calculated for experiments in chapter 4.

B.1 Error estimates for pressure drop measurements in MCIP

The pressure drop measurements were repeated three times for each microchannel with integrated micropillar (MCIP). Data were collected once the flow attained steady state conditions. The uncertainty due to instrumentation error (e_{inst}) was found to be 1.58 % and was derived from the manufacturer's specification sheet. Calibration error was negligible for the pressure transducer. The random errors (e_{rand}) involved in the measurements were obtained by calculating the standard error of the three readings of pressure drop measurements for each MCIP. The net error associated with each reading is given by $e = \sqrt{{e_{inst}}^2 + {e_{rand}}^2}$ and is shown in Table B.1 of this supplementary document.

[1]This appendix has been included as supplementary material for chapter 3 which is submitted for publication in *Microfluidics and Nanofluidics*, August 2012, *In review*

Table B.1 – Uncertainity in pressure measurements at different flow rates in MCIPs.

Arrangement	Error (%)						
	$50(\mu l/min)$	$80(\mu l/min)$	$100(\mu l/min)$	$200(\mu l/min)$	$300(\mu l/min)$	$400(\mu l/min)$	$600(\mu l/min)$
NSq 95-30	-	-	-	1.9	3.2	8.2	4.9
NSq 90-30	3.5	8.1	3.1	2.5	9.7	8.9	-
NSq 80-50	3.9	4.6	2.1	8.7	4.8	-	-
NSq 70-50	1.9	1.9	2.1	2.9	-	-	-
NSq 50-100	3.7	4.3	3.1	4.6	-	-	-
NSt 90-30	-	3.6	8.0	3.8	5.1	5.2	-
NSt 80-50	1.5	2.8	2.5	2.3	2.9	-	-
NSt 70-50	4.0	6.7	6.1	4.1	9.4	-	-
NSt 50-100	2.5	6.4	2.3	6.6	6.4	-	-

Appendix C

Flowchart for Monte Carlo simulation

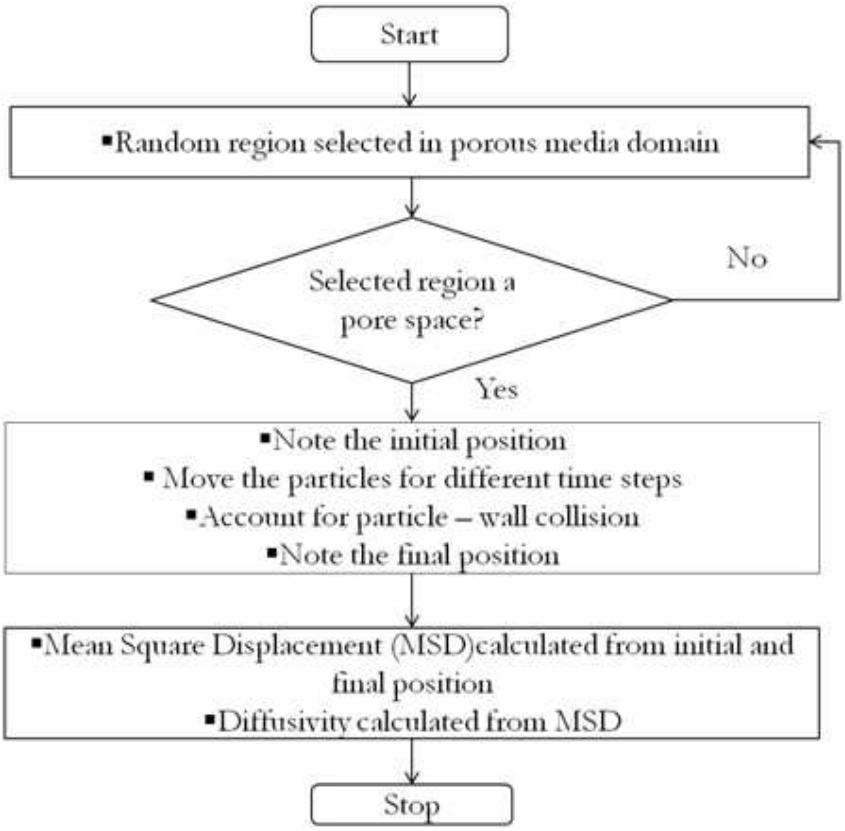

Figure C.1 – Random Walk algorithm for calculating effective diffusivity in a FIB SEM image of SOFC electrode